

2020 Global reassessment of the neutrino oscillation picture

P. F. de Salas,^{1,*} D. V. Forero,^{2,†} S. Gariazzo,^{3,4,‡} P. Martínez-Miravé,^{3,5,§}
 O. Mena,^{3,¶} C. A. Ternes,^{3,4,**} M. Tórtola,^{3,5,††} and J. W. F. Valle^{3,‡‡}

¹*The Oskar Klein Centre for Cosmoparticle Physics, Department of Physics,
 Stockholm University, AlbaNova, 10691 Stockholm, Sweden*

²*Universidad de Medellín, Carrera 87 N° 30 - 65, Medellín, Colombia*

³*Instituto de Física Corpuscular, CSIC-Universitat de València, 46980 Paterna, Spain*

⁴*INFN, Sezione di Torino, Via P. Giuria 1, I-10125 Torino, Italy*

⁵*Departament de Física Teòrica, Universitat de València, 46100 Burjassot, Spain*

Abstract

We present an updated global fit of neutrino oscillation data in the simplest three-neutrino framework. In the present study we include up-to-date analyses from a number of experiments. Concerning the atmospheric and solar sectors, besides the data considered previously, we give updated analyses of IceCube DeepCore and Sudbury Neutrino Observatory data, respectively. We have also included the latest electron antineutrino data collected by the Daya Bay and RENO reactor experiments, and the long-baseline T2K and NO ν A measurements, as reported in the Neutrino 2020 conference. All in all, these new analyses result in more accurate measurements of θ_{13} , θ_{12} , Δm_{21}^2 and $|\Delta m_{31}^2|$. The best fit value for the atmospheric angle θ_{23} lies in the second octant, but first octant solutions remain allowed at $\sim 2.4\sigma$. Regarding CP violation measurements, the preferred value of δ we obtain is 1.08π (1.58π) for normal (inverted) neutrino mass ordering. The global analysis still prefers normal neutrino mass ordering with 2.5σ statistical significance. This preference is milder than the one found in previous global analyses. These new results should be regarded as robust due to the agreement found between our Bayesian and frequentist approaches. Taking into account only oscillation data, there is a weak/moderate preference for the normal neutrino mass ordering of 2.00σ . While adding neutrinoless double beta decay from the latest Gerda, CUORE and KamLAND-Zen results barely modifies this picture, cosmological measurements raise the preference to 2.68σ within a conservative approach. A more aggressive data set combination of cosmological observations leads to a similar preference for normal with respect to inverted mass ordering, namely 2.70σ . This very same cosmological data set provides 2σ upper limits on the total neutrino mass corresponding to $\Sigma m_\nu < 0.12$ (0.15) eV in the normal (inverted) neutrino mass ordering scenario. The bounds on the neutrino mixing parameters and masses presented in this up-to-date global fit analysis include all currently available neutrino physics inputs.

*Electronic address: pablo.fernandez@fysik.su.se

†Electronic address: dvanegas@udem.edu.co

‡Electronic address: gariazzo@to.infn.it

§Electronic address: pamarmi@ific.uv.es

¶Electronic address: omena@ific.uv.es

**Electronic address: chternes@ific.uv.es

††Electronic address: mariam@ific.uv.es

‡‡Electronic address: valle@ific.uv.es

Contents

I. Introduction	2
II. Experimental data	4
A. Solar neutrino experiments and KamLAND	4
B. Reactor neutrino experiments	6
C. Atmospheric neutrino experiments	7
D. Accelerator experiments	9
III. Results from the global fit	11
A. Well-measured oscillation parameters	11
B. The atmospheric angle θ_{23}	12
C. The CP phase δ	13
D. The neutrino mass ordering	14
IV. Bayesian analysis of neutrino oscillation data	16
A. The Bayesian method	16
B. Oscillation parameter results	17
V. Absolute scale of neutrino masses	18
A. The end point of β decay spectra	18
B. Neutrinoless double β decay	19
C. Cosmological probes	20
D. Global results on the neutrino mass scale and mass ordering	21
VI. Summary of the global fit	24
Acknowledgments	28
References	28

I. INTRODUCTION

This paper updates the results from a long ongoing series of global fits to neutrino oscillation data [1–8]*. Neutrino flavor conversion was first observed in solar [11] and atmospheric neutrinos [12]. This discovery led to the Nobel prize in Physics in 2015 [13, 14] and was confirmed by subsequent results from the KamLAND reactor experiment [15] as well as long baseline accelerator experiments. These were crucial to identify neutrino oscillations as *the* explanation of the

* For the results obtained by other groups see Refs. [9, 10].

Parameter	Main contribution from	Other contributions from
Δm_{21}^2	KamLAND	SOL
$ \Delta m_{31}^2 $	LBL+ATM+REAC	-
θ_{12}	SOL	KamLAND
θ_{23}	LBL+ATM	-
θ_{13}	REAC	(LBL+ATM) and (SOL+KamLAND)
δ	LBL	ATM
MO	(LBL+REAC) and ATM	COSMO and $0\nu\beta\beta$

TABLE I: The main contribution to each of the oscillation parameters from the different classes of experiments.

solar neutrino problem and the atmospheric neutrino anomaly[†]. In the simplest three-neutrino scenario, the probability for a neutrino to oscillate between flavors is described by six parameters, Δm_{21}^2 , $|\Delta m_{31}^2|$, θ_{12} , θ_{13} , θ_{23} and δ . In addition, there are two possible mass orderings (MO) for neutrinos, according to the positive or negative sign of Δm_{31}^2 . In the first case, we talk about normal ordering (NO), and in the latter, about inverted ordering (IO). The parameters are measured by different types of experiments, i.e. in solar experiments (SOL), in atmospheric experiments (ATM), in the long-baseline reactor experiment KamLAND, in short-baseline[‡] reactor experiments (REAC) and in long-baseline accelerator experiments (LBL). Moreover, data from cosmological observations (COSMO) can constrain the absolute mass scale, giving an indirect contribution to the determination of the neutrino mass ordering. If neutrinos turn out to be Majorana particles, the non-observation of $0\nu\beta\beta$ would also provide complementary information on the absolute neutrino mass scale and disfavor inverted neutrino mass ordering.

In Tab. I we summarize the sensitivity of the various experiment types in probing each of the oscillation parameters. Since many of the parameters are measured by several classes of experiments, a combined or global fit of all data will give more precise results than a measurement of a single experiment on its own. Performing such global analysis is precisely the purpose of this study. The paper is structured as follows: in Sec. II we present the analysis of each class of experiments, focusing on solar experiments and KamLAND, short-baseline reactor experiments, atmospheric experiments and, finally, long-baseline accelerator experiments. Next, we show the results from our global fit to neutrino oscillation data, following a frequentist approach in Sec. III, and a Bayesian approach in Sec. IV. In Sec. V we discuss the effects of the inclusion of non-oscillation data sets and present our final results on the neutrino mass ordering. Finally, we summarize all our results in Sec. VI.

[†] Other mechanisms, such as magnetic moments [16–18] or non-standard interactions [19–21] could be present only at a sub-leading level [7], for recent analyses see, e.g. [22, 23].

[‡] Here, we use the term short-baseline for baselines of the order of 1 km. We will not discuss the searches for light sterile neutrinos. We refer the interested reader to Refs. [24–31].

II. EXPERIMENTAL DATA

In this section we discuss the experimental results included in our global fit with more detail. We dedicate one subsection to describe each class of experiments, discussing the main details of the data sets analyzed. The results of the oscillation analysis in each sector are presented as well.

A. Solar neutrino experiments and KamLAND

Solar neutrinos are produced in thermonuclear reactions in the interior of the Sun when burning hydrogen into helium. The main nuclear chains producing neutrinos are the so-called proton-proton (pp) chain and the CNO cycle. Neutrinos are produced in different reactions with energies ranging from 0.1 to 20 MeV. Our solar oscillation analysis includes data from all past and present solar neutrino oscillation experiments. We use the total rate measurements performed at the radiochemical experiments Homestake [32], GALLEX/GNO [33] and SAGE [34], the low-energy ^7Be neutrino data from Borexino [35, 36], as well as the zenith-angle or day/night spectrum from phases I–IV in Super-Kamiokande [37–40].[§] Finally, we also include the last results from the Sudbury Neutrino Observatory (SNO), combining the solar neutrino data from the three phases of the experiment [43]. As in previous works, we have considered the low metallicity version of the standard solar model, labeled as AGSS09 [44]. The result of our combined analysis of solar neutrino oscillation data is shown in Fig. 1.

The solar neutrino oscillation parameters were also measured at the KamLAND experiment [45–47]. This long-baseline reactor neutrino experiment used a single detector to detect neutrinos from 56 nuclear reactors at an average distance of 180 km. This long distance made KamLAND sensitive to the values of the mass splitting Δm_{21}^2 indicated by the solar data analysis. In our global fit, we include KamLAND data as presented in Ref. [46]. The result of our analysis is shown together with the result from the analysis of solar neutrino oscillation data in Fig. 1. As can be seen in the figure, the solar experiments provide a more precise measurement of the solar mixing angle, while KamLAND gives a better determination of the solar mass splitting. Note that, since KamLAND is mostly sensitive to $\sin^2 2\theta_{12}$, using KamLAND data alone, we would obtain a second minimum in the upper octant of $\sin^2 \theta_{12}$. This solution is excluded when combining with solar neutrino data, sensitive to $\sin^2 \theta_{12}$ through the observation of the adiabatic conversion in the solar medium. Note, however, that the upper-octant solution may emerge in the presence of non-standard interactions [21, 48, 49].

Recently, the final results from Super-Kamiokande IV were presented, including 2970 days of data taking [42]. These results are particularly important due to two factors. First of all, the ratio

[§] The measurement of the CNO solar neutrino flux, recently presented by Borexino [41] is not expected to have an impact on the determination of the oscillation parameters and, hence, is not included in this analysis. Regarding the latest solar results from Super-Kamiokande [42], although they are also not included in this analysis, their implications are discussed.

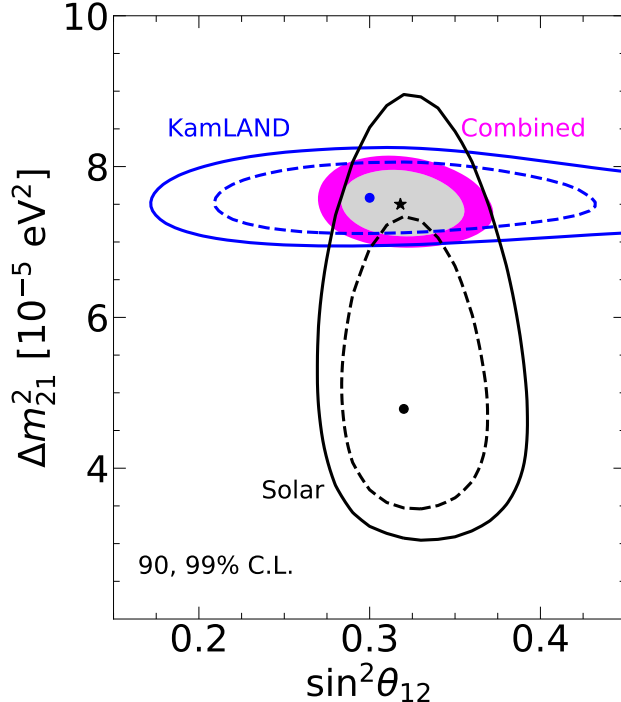


FIG. 1: 90 and 99% C.L. (2 d.o.f.) allowed regions in the $\sin^2 \theta_{12} - \Delta m_{21}^2$ plane obtained from the analysis of solar neutrino experiments (black lines), from KamLAND (blue lines) and from the combined analysis (colored regions). The best fit values are indicated with dots for the independent analyses and with a star for the combined solar + KamLAND analysis. The reactor mixing angle θ_{13} has been marginalized over without further constraint from short-baseline reactor experiments.

between the data and the unoscillated prediction has shifted upwards with respect to previous results. Secondly, a smaller value of the day-night asymmetry has been reported. According to the internal analysis of the collaboration, these two facts contribute equally, in terms of $\Delta\chi^2$, to shift the preferred value of Δm_{21}^2 to higher values. As a result, the previous tension between solar experiments and KamLAND in the determination of this parameter is significantly reduced. Despite their relevance for the consolidation of the neutrino oscillations picture, these results are not expected to have a large impact in global fits, since the preferred value of Δm_{21}^2 after the combination of all data sets is dominated by KamLAND [¶].

The best fit value obtained by solar experiments, $\Delta m_{21}^2 = 4.8 \times 10^{-5} \text{ eV}^2$, is excluded by KamLAND with a high confidence level. However, the regions overlap above 90% C.L. Moreover, notice that the solar experiments and KamLAND show also a marginal sensitivity to θ_{13} , which can be enhanced at the combined analysis [6, 50]. In order to generate Fig. 1, we have marginalized over θ_{13} , without taking any constraint from short baseline reactor data, which we discuss in the next subsection.

[¶] In addition, publicly available information does not allow one to precisely reproduce the results reported [42] and hence these constraints are not included in our analysis due to the impossibility of accounting properly for these measurements.

B. Reactor neutrino experiments

Besides KamLAND, there are several other reactor neutrino oscillation experiments. Here, we use data coming from the reactor experiments RENO [51] and Daya Bay [52]. Unlike KamLAND, they lie quite close to the nuclear power plants. This makes them sensitive to θ_{13} and Δm_{31}^2 **. Using current reactor neutrino data, it was shown that there is also some sensitivity to the solar parameters [54]. Note that these, however, are not competitive with the results coming from KamLAND and solar experiments and therefore we fix in our analyses the solar parameters to the ones measured by those experiments, as discussed in the previous section.

The Reactor Experiment for Neutrino Oscillation (RENO) is a neutrino oscillation experiment located at the Hanbit Nuclear Power Plant (South Korea), that has been taking data since August 2011. Two functionally identical 16 ton detectors placed at 294 m and 1383 m from the centerline of the antineutrino sources, detect electron antineutrinos produced by six pressurized water reactors (all equally distributed in space along a 3 km line), each with output thermal powers of 2.6 GW_{th} or 2.8 GW_{th}. The average relative fission fractions for these reactor cores can be found in Ref. [55]. In the most recent publication [56], the RENO collaboration reported results that correspond to 2900 days of data taking, updating their former findings [51]. From the observation of electron antineutrino disappearance, RENO reported a value for the reactor mixing angle of $\sin^2(2\theta_{13}) = 0.0892 \pm 0.0063$, and a value of $|\Delta m_{ee}^2| = (2.74 \pm 0.12) \times 10^{-3} \text{ eV}^2$ for the observed neutrino mass squared difference. In our analysis, we consider antineutrino events (background subtracted) at the near and far detectors, as reported by RENO [56], distributed along 26 energy bins in prompt energy, ranging from 1.2 MeV to 8.0 MeV. A total of nine systematical uncertainties, accounting for reactor-flux uncertainties $\sigma_r = 0.9\%$ (correlated between detectors), uncorrelated detection uncertainty $\sigma_{du} = 0.21\%$ [55, 57], and an overall normalization uncertainty $\sigma_o = 2\%$, have been included in the analysis. In the calculation of the signal events, a Gaussian energy smearing was assumed to account for the detector energy resolution with a width $\sigma_E/E \approx 7\%/\sqrt{E[\text{MeV}]}$ [55].

The Daya Bay Reactor Neutrino experiment analyzes the antineutrino flux produced by six reactor cores at the Daya Bay and Ling Ao nuclear power plants. The electron antineutrino oscillation probability is measured by eight identical antineutrino detectors (ADs). Two detectors are placed in each of the two near experimental halls of the experiment (EH1 and EH2), while the remaining four are located at the far experimental hall (EH3). Detailed studies on the antineutrino flux and spectra have been performed in order to determine the fission fractions (see Tab. 9 in Ref. [58]) as well as the thermal power (see Tab. I in Ref. [59]). Baseline distances range in $\sim 0.3 - 1.3$ km for the near experimental halls and $\sim 1.5 - 1.9$ km for the far hall. The Daya Bay collaboration analyzed data collected after 1958 days of running time [52] and reported the measurements $\sin^2(2\theta_{13}) = 0.0856 \pm 0.0029$ and $|\Delta m_{ee}^2| = (2.522_{-0.070}^{+0.068}) \times 10^{-3} \text{ eV}^2$. To obtain the oscillation parameters, our analysis uses the number of antineutrino events after background

** Actually, short-baseline reactor experiments are sensitive to the effective mass splitting $\Delta m_{ee}^2 = \cos^2 \theta_{12} \Delta m_{31}^2 + \sin^2 \theta_{12} \Delta m_{32}^2$ [53].

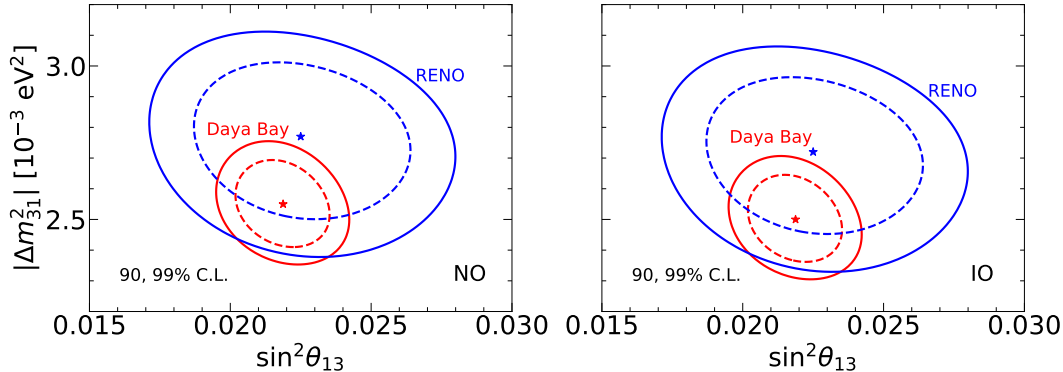


FIG. 2: 90 and 99% C.L. (2 d.o.f.) allowed regions in the $\sin^2 \theta_{13} - \Delta m_{31}^2$ plane for RENO (blue) and Daya Bay (red). The best fit values are indicated by stars. The left (right) panels correspond to NO (IO).

subtraction, considering the ratios of EH3 to EH1 and EH2 to EH1. Regarding the statistical methods, the Daya Bay collaboration has followed three different approaches (covariant approach, nuisance parameters and a hybrid approach). Consistent results can be obtained with the three methods and we have chosen to use nuisance parameters in our analysis. The uncertainties arising from the power and fission fractions at each of the 6 nuclear reactors are encoded in these nuisance parameters ($\sigma_r = 0.2\%$ and $\sigma_{frac} = 0.1\%$). In addition, characteristics of each detector, such as the differences in the running time or the efficiencies, have been accounted for in the simulation. Other sources of uncertainties, such as shifts in the energy scale ($\sigma_{scale} = 0.6\%$), have also been included.

The results of our analyses of short-baseline reactor data are shown in Fig. 2. As can be seen in the figure, there is a total overlap between the parameter regions determined by RENO and Daya Bay, although the latter clearly dominates the measurement of the relevant oscillation parameters. Note also that our results are almost identical for normal and inverted mass spectra, since these experiments are not sensitive to the mass ordering.

C. Atmospheric neutrino experiments

When cosmic rays collide with particles in the Earth's atmosphere, they start a particle shower which eventually creates the atmospheric neutrino flux. The energy of ν_μ and ν_e (and their antiparticles) produced in the atmosphere can range from a few MeV up to roughly 10^9 GeV, although only events up to ~ 100 TeV are currently detectable. The energy of the atmospheric neutrinos relevant to oscillation studies, however, ranges from ~ 0.1 GeV to ~ 100 GeV. In our global fit we include data from Super-Kamiokande [60] and from IceCube DeepCore [61, 62]. Since the largest part of the atmospheric neutrino flux is composed by ν_μ and $\bar{\nu}_\mu$, and given that it is more difficult to identify electrons in the detector, the main channel used in current atmospheric neutrino experiments is $\nu_\mu \rightarrow \nu_\mu$, which makes them mostly sensitive to the oscillation parameters θ_{23} and Δm_{31}^2 . Note, however, that the Super-Kamiokande experiment also detected a large sample of

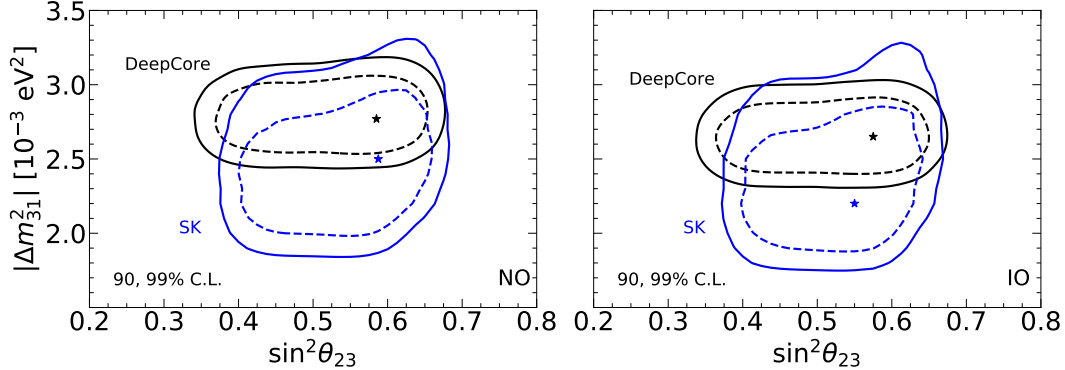


FIG. 3: 90 and 99% C.L. (2 d.o.f.) allowed regions at the $\sin^2 \theta_{23} - \Delta m_{31}^2$ plane for NO (left) and IO (right), obtained from the analyses of Super-Kamiokande (SK) atmospheric (blue) and DeepCore (black) data. The best fit values are indicated by stars.

electron events from ν_e appearance [60, 63]. The analysis of these results, however, can not be precisely performed outside the experimental collaboration. As a result, we do not analyze Super-Kamiokande atmospheric data ourselves, but only include the latest χ^2 -table made available by the collaboration [64]. The Super-Kamiokande collaboration recently presented an updated analysis of atmospheric neutrino data [42]. This new analysis slightly prefers the region with $\sin^2 \theta_{23} < 0.5$ and shows a weaker preference for the normal neutrino mass ordering than the data set included in our analysis. However, the collaboration has not released the new χ^2 -tables and, therefore, we can not include the new atmospheric results in our present analysis.

For the current global fit, we update our analysis of DeepCore data. In addition to track-like events, the released experimental data now includes also shower-like events, increasing the number of events from roughly 6000 [65] to around 20000 [61, 62]. The data analyzed correspond to 3 years of observations of the full sky, from April 2012 to May 2015. The details of the analysis are described in Ref. [62], and the full data set can be downloaded from Ref. [66]. Two data samples are provided: Sample A and Sample B, corresponding to the same data taking period but different cuts. For this analysis we have chosen Sample A. Several sources of systematic uncertainties are included in our analysis. They can be divided into detector-related and flux-related uncertainties. We account for neutrino scattering and absorption in the ice, and include several uncertainties related to the optical efficiencies. Concerning the atmospheric neutrino flux, we include systematic uncertainties on the ratio of neutrinos to antineutrinos, the ratio of electron to muon neutrinos, the spectral index, the ratio of vertically to horizontally incoming neutrinos and an overall normalization. The results of our analysis are depicted in Fig. 3, together with the ones from Super-Kamiokande. As in the reactor case, the regions allowed by the two experiments totally overlap. However, one can see that the mixing angle is slightly better measured by Super-Kamiokande, while DeepCore provides a more stringent result on the atmospheric mass splitting.

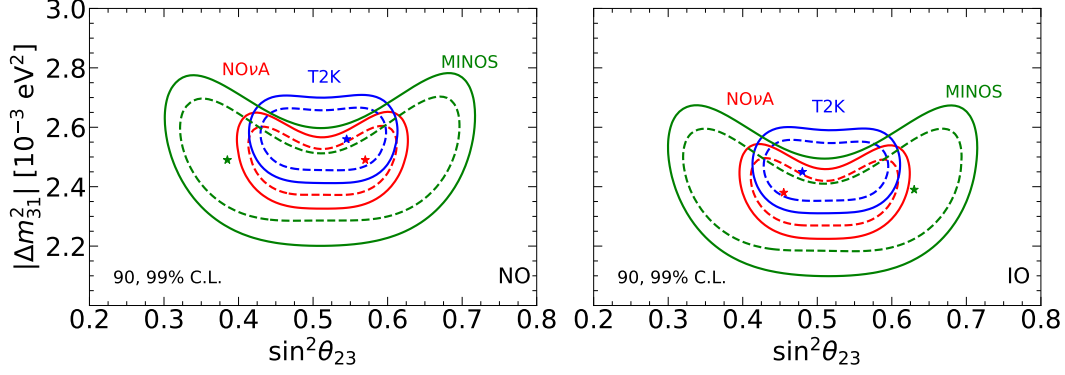


FIG. 4: 90 and 99% C.L. (2 d.o.f.) allowed regions in the $\sin^2 \theta_{23} - \Delta m_{31}^2$ plane for NO (left) and IO (right), obtained from the analyses of T2K (blue), NO ν A (red) and MINOS (green) data. The best fit values are indicated by stars.

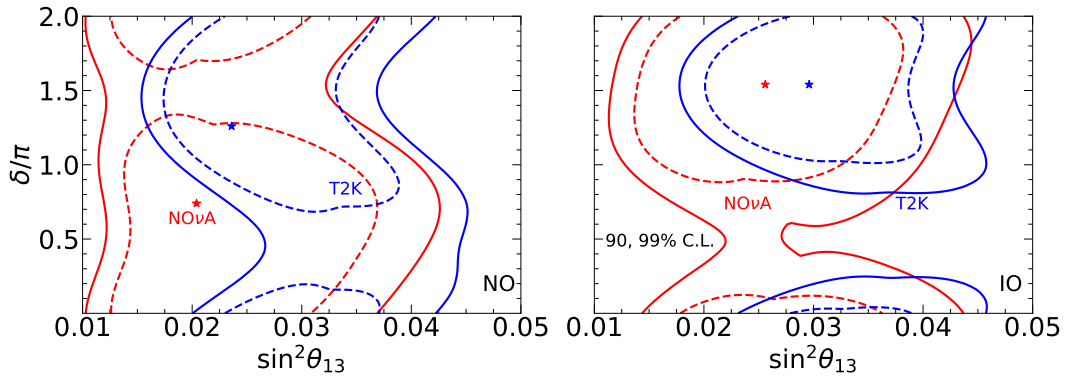


FIG. 5: 90 and 99% C.L. (2 d.o.f.) allowed regions in the $\sin^2 \theta_{13} - \delta$ plane for NO (left) and IO (right), obtained from the analyses of T2K (blue) and NO ν A (red) data. The best fit values are indicated by stars.

D. Accelerator experiments

Long-baseline accelerator neutrino experiments measure neutrinos which are created in particle accelerators. They originate in meson decays. The mesons, typically pions and kaons, are created in the accelerator and then focused into a beam. Next, they decay into muon-neutrinos, while a beam dump absorbs the ones which do not decay. Using different polarities of the focusing horns one can separate mesons from antimmesons, resulting in a mostly pure beam of neutrinos or antineutrinos. Note, however, that creating a really pure beam is not possible, and there will always be a background contamination of so-called “wrong-sign” neutrinos. The long-baseline experiments consist of two detectors, one near detector measuring the initial neutrino flux, close to the accelerator complex, and a far detector measuring the oscillated neutrino flux. Long-baseline experiments measure the appearance of ν_e from the initial ν_μ flux, and also the disappearance of ν_μ . This makes them sensitive to the oscillation parameters Δm_{31}^2 , θ_{23} , θ_{13} , δ and, in principle, also to the neutrino mass ordering. In our global fit, we use data from several long-baseline experiments: NO ν A [67], T2K [68], MINOS [69] and K2K [70].

The T2K collaboration has presented an updated analysis of neutrino and antineutrino data, corresponding to an exposure at Super-Kamiokande of 1.97×10^{21} protons on target (POT) in neutrino mode and 1.63×10^{21} POT in antineutrino mode. Data have been collected from January 2010 until June 2018. T2K observed 318 (137) muon (anti-muon) events and 94 (16) electron (positron) events. In addition, 14 electron events where also a pion is produced were recorded. These results improve their former ones [71–73], allowing them now to exclude CP-conserving values of δ at close to 3σ confidence level.

On the other hand, NO ν A has reached 13.6×10^{20} POT in neutrino mode [74] and 12.5×10^{20} POT in antineutrino mode. NO ν A finds 212 (105) muon (anti-muon) events and 82 (33) electron (positron) events. The events in antineutrino mode constitute the first ever significant observation of $\bar{\nu}_e$ appearance in a long baseline experiment [75]. Unlike T2K, the latest neutrino and antineutrino NO ν A data prefer values of the CP-violating phase δ close to 0.8π for normal ordering, in tension with the T2K result.

In order to perform our analysis, we extract the relevant data for each experiment from the corresponding reference. We simulate the signal and background rates using the GLoBES software [76, 77]. For the energy reconstruction we assume Gaussian smearing. We include bin-to-bin efficiencies, which are adjusted to reproduce the best-fit spectra reported in the corresponding references. Finally, for our statistical analysis we include systematic uncertainties, related to the signal and background predictions, which we minimize over. The results of our analysis (without a prior on θ_{13}) are presented in Figs. 4 and 5. We find that T2K and NO ν A measure the atmospheric parameters θ_{23} and $|\Delta m_{31}^2|$ rather well and with similar sensitivity. Note, however, that T2K shows a slightly better sensitivity to θ_{13} and δ for inverted neutrino mass ordering, as indicated by the 90% C.L. closed regions in the right panel of Fig. 5. For normal neutrino mass ordering, both experiments show similar sensitivity to δ , although T2K provides a better measurement of the mixing angle θ_{13} than NO ν A. In any case, these results are not competitive with short-baseline reactor experiments, discussed above. Focusing on the determination of δ , the aforementioned tension between T2K and NO ν A results for normal ordering is clearly visible in the left panel of Fig. 5. Note that here we are not imposing any prior on θ_{13} , as the experimental collaborations do, and yet, the mismatch between both samples is quite evident. We shall discuss in more detail this tension in the measurement of δ and its consequences on the determination of the neutrino mass ordering in Sec. III.

We also show the results from our analysis of MINOS data [78, 79], which still contributes to the determination of $|\Delta m_{31}^2|$, as seen in Fig. 4. Unfortunately, in this case there is no sensitivity to θ_{13} and δ . The same applies to the pioneering K2K experiment [80], included in our global fit as well, but with a sensitivity to the oscillation parameters which has been overcome by the more recent long-baseline accelerator experiments.

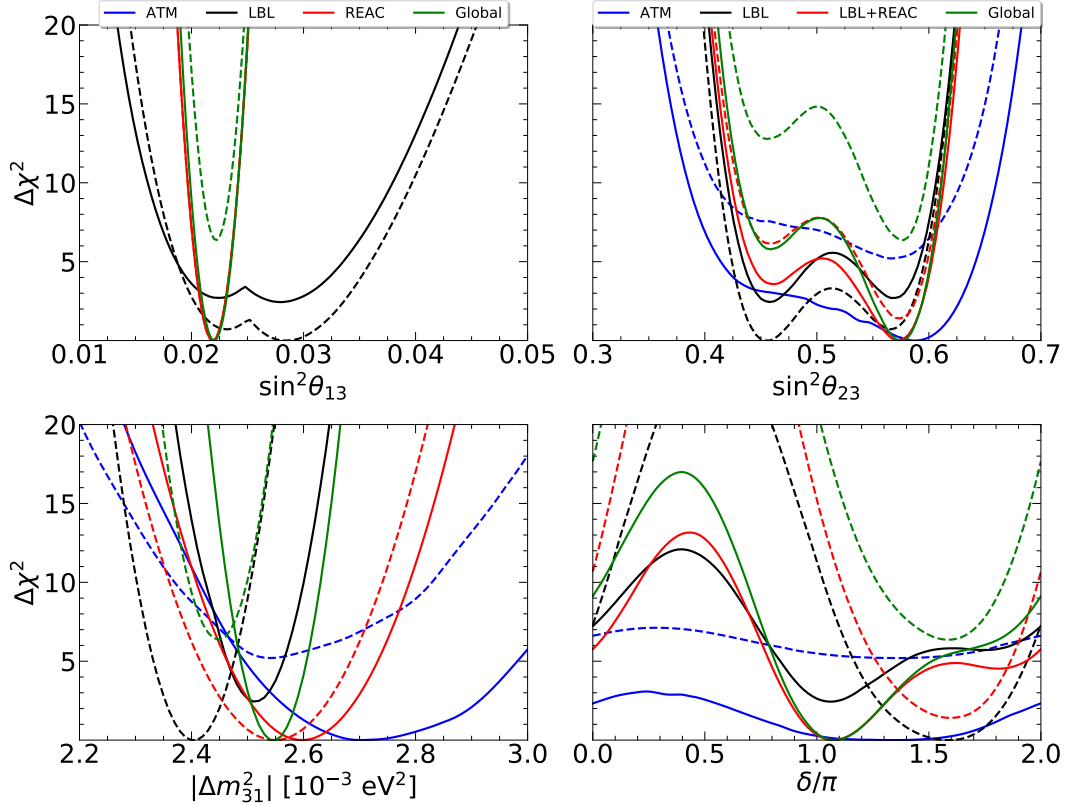


FIG. 6: $\Delta\chi^2$ profiles obtained from the combination of all ATM data (blue), all LBL data (black) and global data (green). Red lines correspond to the analysis of all REAC data in the panels of the parameters measured by reactor experiments directly and to LBL+REAC data for the parameters where reactors enter only via correlations. The solid (dashed) lines correspond to NO (IO). The profiles are calculated with respect to the global minimum for each data sample, corresponding to normal ordering in all cases.

III. RESULTS FROM THE GLOBAL FIT

In the previous section, we have presented the individual results of our neutrino data analysis, obtained sector-by-sector. In this section, we shall describe the results obtained by combining all previous data into our global neutrino oscillation fit. We will first briefly discuss the main contributions to the well-measured parameters, and then enter into more detail in the discussion of the remaining unknowns of the three-neutrino picture.

A. Well-measured oscillation parameters

So far the solar parameters θ_{12} and Δm_{21}^2 have only been measured by KamLAND and the solar neutrino experiments, and they have already been discussed in Sec. II A. After combining with data from other experiments the determination of the solar parameters improves further, due to a better determination of θ_{13} , but the effect is not very visible. The future reactor experiment JUNO is expected to measure the solar parameters with great precision [81]. In contrast, the measurement

of the remaining oscillation parameters emerge from the combinations of several data sets, as seen in Fig. 6. From these four parameters, only θ_{13} and Δm_{31}^2 have been already measured with good precision at oscillation experiments. Concerning the reactor mixing angle, if we compare the regions in Fig. 2 with those in Fig. 5, one sees that the measurement of θ_{13} is clearly dominated by reactor experiments. The contribution from other experiments to this result is negligibly small. This behavior can also be appreciated in the upper left panel of Fig. 6, where we see that the combination of global data (green lines) is basically equivalent to the combination of reactor data (red lines). Regarding the absolute value of the atmospheric mass splitting, $|\Delta m_{31}^2|$, we see from Figs. 2, 3 and 4 that its determination comes mainly from long-baseline accelerators and from Daya Bay, although the determination by atmospheric experiments is still important, as indicated in the lower left panel of Fig. 6. Comparing the lines corresponding to the analyses of long-baseline (black), reactor (red) and atmospheric data (blue) together with the result from the global fit (green lines) we find that, unlike the case of $\sin^2 \theta_{13}$, all experiments contribute significantly to this measurement.

B. The atmospheric angle θ_{23}

Next, we discuss the determination of the atmospheric mixing angle, θ_{23} . Accelerator and atmospheric oscillation experiments measure the disappearance of muon (anti)neutrinos and are mainly sensitive to $\sin^2 2\theta_{23}$. Therefore, they can not resolve the octant of the angle: in other words, they can not determine if $\sin^2 \theta_{23} > 0.5$ or $\sin^2 \theta_{23} < 0.5$. However, due to matter effects in the neutrino trajectories inside the Earth, this degeneracy is slightly broken for atmospheric neutrino oscillation experiments, see the blue lines in the upper right panel of Fig. 6. Also, the quantity $\sin^2 \theta_{23}$ enters directly in the appearance channels of these experiments and, hence, the degeneracy can be further broken when including the electron neutrino samples in the fit. Analyzing the data from long-baseline accelerators, we find two essentially degenerate solutions for $\sin^2 \theta_{23}$ for both mass orderings, as indicated by the black lines in the upper right panel of Fig. 6. The best fit is obtained for $\sin^2 \theta_{23} = 0.46$, but a local minimum appears at $\sin^2 \theta_{23} = 0.57$ with $\Delta\chi^2 \approx 0.3$ (0.7) for normal (inverted) ordering. Although θ_{23} is not measurable in reactor neutrino experiments, their data help in the determination of θ_{23} by breaking a degeneracy between θ_{23} and θ_{13} , as indicated by the red lines in the upper right panel of Fig. 6, obtained from the combination of reactor and long-baseline accelerator data. In this case, the best fit value is obtained in the upper octant for both orderings. This effect can be further appreciated in Figure 7, showing the regions obtained from several combinations of data sets in the $\sin^2 \theta_{23}$ - $\sin^2 \theta_{13}$ plane at 90 and 99% C.L. for two degrees of freedom. There, one sees how the combination of all accelerator data (black lines in the figure) prefers a rather large value of $\sin^2 \theta_{13}$. The combination of LBL with atmospheric data (blue) does not improve the determination of θ_{13} , but shifts the best fit value of the analysis (indicated by the blue square) towards smaller values, as preferred by reactor data. Note also that this combined analysis shifts the best fit value of $\sin^2 \theta_{23}$ to the second octant. A more distinctive

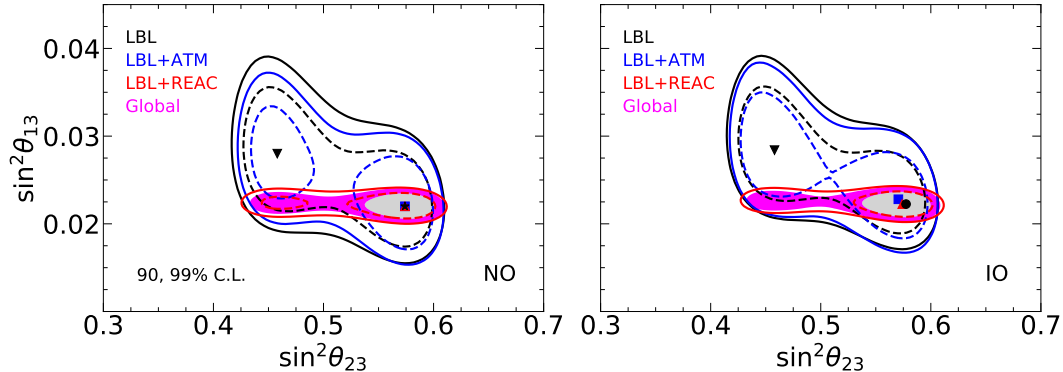


FIG. 7: Allowed regions in the $\sin^2 \theta_{23}$ – $\sin^2 \theta_{13}$ plane from several combinations of data sets: LBL (black lines), LBL+ATM (blue), LBL+REAC (red) and global analysis (colored regions). The down-triangle, square and up-triangle correspond to the best fit values obtained from the combination of data sub-sets, while the black star (left panel) and black dot (right panel) denote the best value obtained from the global fit, for normal and inverted ordering, respectively.

feature appears when combining LBL with reactor data. As expected, this combination results in a much more restricted range for θ_{13} and, therefore, the partial breaking of the θ_{23} – θ_{13} degeneracy, arising from the LBL appearance data, see the red lines in Fig. 7. Finally, when combining all data, we obtain the green lines in Fig. 6 and the colored regions in Fig. 7. There, one sees that the effect from both combinations (LBL+ATM and LBL+REAC) is indeed very relevant for the determination of the octant of the atmospheric angle. After combining all data samples, we obtain the best fit value of θ_{23} in the upper octant, with lower octant solutions slightly disfavored with $\Delta\chi^2 \geq 5.8$ (6.4) for normal (inverted) mass ordering. Maximal atmospheric mixing is disfavoured with $\Delta\chi^2 = 7.8$ (8.5) for normal (inverted) ordering^{††}.

C. The CP phase δ

We now discuss the measurement of the CP-violating phase, δ . This phase induces opposite shifts in the $\nu_\mu \rightarrow \nu_e$ and $\bar{\nu}_\mu \rightarrow \bar{\nu}_e$ oscillation probabilities and, therefore, information on this parameter can be obtained by analyzing neutrino and antineutrino oscillation data in the appearance channels. Note, however, that the separate analysis of neutrino and antineutrino channels can not provide, at present, a sensitive measurement of δ [82]. The CP phase can therefore be measured by the long-baseline accelerator experiments T2K and NO ν A, and also by Super-Kamiokande atmospheric neutrino data, see the black and blue lines in the lower right panel of Fig. 6. In addition to Fig. 6, in Fig. 8 we show the $\Delta\chi^2$ profiles for the CP-violating phase δ as obtained from the analysis of data from T2K (blue) and NO ν A (red), the combination of all long-baseline data (black) and the result from the global fit (green). For normal neutrino mass ordering (left panel), a tension

^{††} Note that the preference for the second octant, as well as the rejection against maximal atmospheric mixing, could change when including the latest Super-Kamiokande results [42], not publicly available yet.

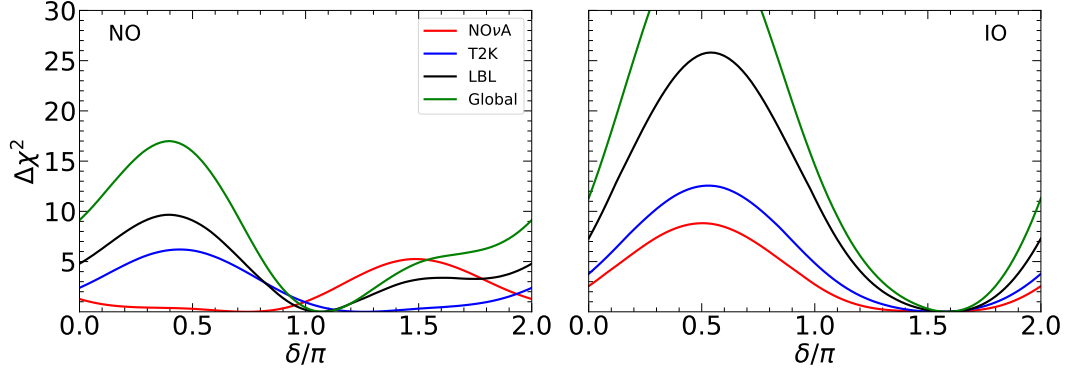


FIG. 8: $\Delta\chi^2$ profiles for δ obtained from the analysis of NO ν A (red), T2K (blue), all long-baseline data (black) and from the global fit (green).

arises between the determinations of δ obtained from T2K and NO ν A data^{‡‡}. Indeed, the analysis of NO ν A results shows a preference for $\delta \approx 0.8\pi$, disfavoring the region around $\delta \approx 1.5\pi$, where the best fit value for T2K is found. This does not happen for inverted ordering (right panel), for which NO ν A shows better sensitivity to δ and also an excellent agreement with T2K. Note that this behavior is due to the antineutrino data sample collected by NO ν A, and it is the reason why our sensitivity to δ in the current global fit is worse than it was in Ref. [1]. The inclusion of reactor data can help to improve the determination of δ , due to the existing correlation between the CP phase and θ_{13} . This is illustrated in Fig. 6 and in the upper panels of Fig. 9. From the global combination, we obtain the best fit value for the CP phase at $\delta = 1.08\pi$ (1.58π) for NO (IO). The CP-conserving value $\delta = 0$ is disfavored with $\Delta\chi^2 = 9.1$ (11.3). However, the other CP-conserving value, $\delta = \pi$, remains allowed with $\Delta\chi^2 = 0.4$ in NO, while it is excluded with $\Delta\chi^2 = 14.6$ in IO.

D. The neutrino mass ordering

Finally, in this subsection, we present the results of our present analysis on the neutrino mass ordering issue. Combining all neutrino oscillation data, we obtain a preference for normal mass ordering with respect to the inverted one with a value of $\Delta\chi^2 = 6.4$. This corresponds to a 2.5σ preference in favor of NO. This preference comes from several contributions, which we shall discuss in the following. Our independent analyses of NO ν A and T2K data do not show a particular preference for any mass ordering, since we obtain $\Delta\chi^2 \approx 0.4$ in favor of NO in both cases. Such a small value is expected, due to the rather small matter effects present in the neutrino propagation over the corresponding baselines. However, after combining all the long-baseline accelerator data, we find that IO is preferred with 2.4 units in $\Delta\chi^2$. This result appears as a consequence of the tension in the measurement of δ by T2K and NO ν A, as discussed in the previous subsection. Since the tension appears only in normal ordering, the minimum χ^2 from the combined long-baseline

^{‡‡} This tension has been recently discussed in Refs. [9] and [83].

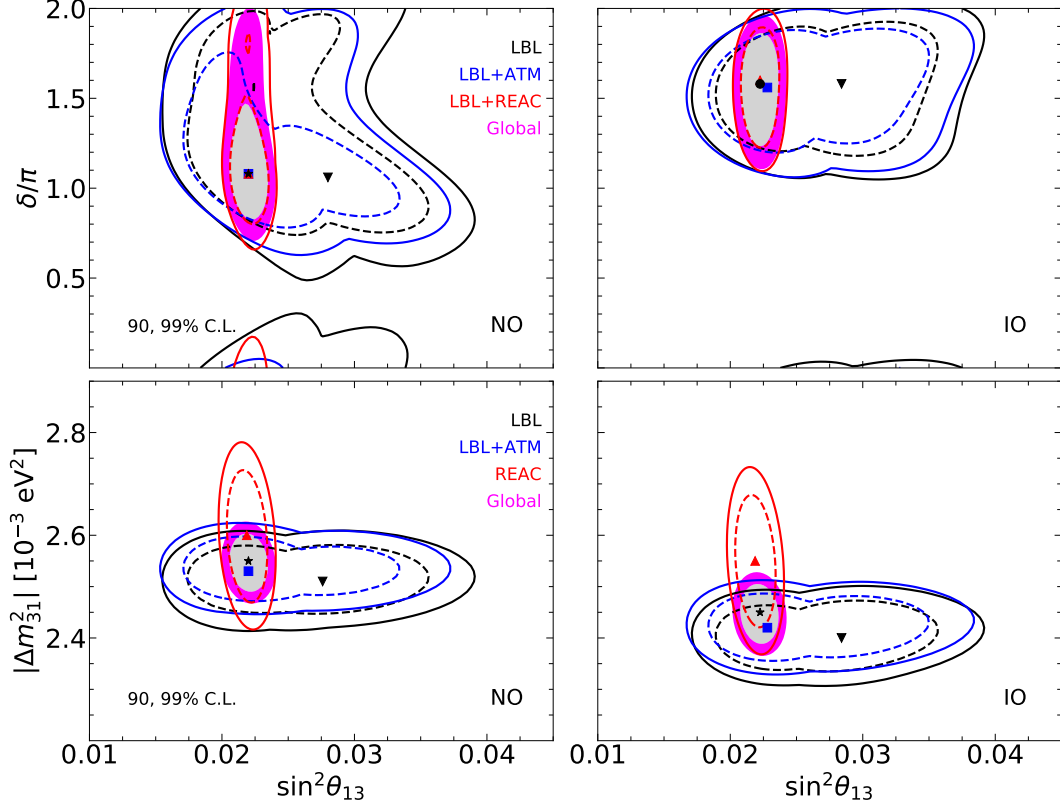


FIG. 9: Allowed regions in the $\sin^2\theta_{13}$ - δ and $\sin^2\theta_{13}$ - Δm_{31}^2 planes from several data-set combinations: long-baseline accelerator experiments (black lines), accelerator and atmospheric data (blue), accelerator and reactor data (red, upper panels), reactor data (red, lower panels) and global analysis (colored regions). The down-triangle, square and up-triangle correspond to the best fit values obtained from the combination of data sub-sets, while the black star (left panel) and black dot (right panel) denote the best fit value obtained from the global fit for normal and inverted ordering, respectively.

analysis for this ordering is worse than the sum of the individual T2K and NO ν A fits. If we now perform a combined analysis of accelerator and reactor data, we obtain a preference for NO with $\Delta\chi^2 = 1.4$. The improved status of normal mass ordering comes from the difference in the measurements of Δm_{31}^2 in accelerator and reactor experiments. As shown in Fig. 6 and in the lower panels of Fig. 9, the values of Δm_{31}^2 preferred by accelerator and reactor experiments show a better agreement for normal ordering than for the inverted one. On the other hand, the atmospheric neutrino results from the Super-Kamiokande and DeepCore experiments show some sensitivity to the neutrino mass ordering on their own. From Super-Kamiokande data alone (neither imposing a prior on θ_{13} nor combining with data from reactor experiments), there is already a preference for normal mass ordering with $\Delta\chi^2 \approx 3.5$, while DeepCore gives $\Delta\chi^2 \approx 1.0$. Combining the atmospheric neutrino results with long-baseline accelerator data, the preference for normal ordering is $\Delta\chi^2 = 3.6$. From Fig. 7 we also notice that, after this combination, the measurement of Δm_{31}^2 agrees better with the reactor one than in the case of long-baseline data alone. However, while the best fit values for normal ordering nearly coincide, there is still a small tension in inverted

ordering. Therefore, after the global combination with data from reactor experiments, we obtain the final preference of $\Delta\chi^2 = 6.4$, corresponding to a significance of 2.5σ . As for the CP phase δ , the current preference for normal mass ordering is lower than reported in Ref. [1]. The explanation is the same as before, namely the tension in the combined analysis of T2K and NO ν A for normal mass ordering, due to the different preferred values for δ . Therefore, any development on this tension will affect the sensitivity of neutrino oscillation data to the mass ordering^{§§}.

IV. BAYESIAN ANALYSIS OF NEUTRINO OSCILLATION DATA

In this section we turn to the discussion of our Bayesian analysis of neutrino oscillation data.

A. The Bayesian method

In order to perform a Bayesian analysis of neutrino oscillation data, we convert the χ^2 functions described in the previous sections into a likelihood, using the expression

$$\ln \mathcal{L} = -\frac{\chi^2}{2}. \quad (1)$$

The analysis is performed using `MontePython` [84, 85] for the computation of the likelihoods and running the Markov Chain Monte Carlo (MCMC) simulations. `MontePython` is also used to post-process the MCMC outputs and obtain the marginalized posteriors and credible intervals. Where used, Bayesian evidences (Z) are computed by means of `MCEvidence` [86]. We checked that `MCEvidence` provides accurate estimates of the Bayesian evidences using the nested sampling code `PolyChord` [87, 88], which is more reliable in case of multivariate distributions but requires longer computation times. The Bayesian evidences are used in the calculation of the Bayes factors $B_{\text{NO,IO}} = Z_{\text{NO}}/Z_{\text{IO}}$, necessary to compare the NO and IO models and decide which of the two is preferred. The significance in favor of the preferred model is derived according to Gaussian probabilities as explained in [89, 90].

When considering neutrino mass bounds, discussed in the following section, the lightest neutrino mass, m_{lightest} , is varied in the analyses using a logarithmic prior in the range $[10^{-3}, 10]$ eV when computing the mass ordering preference [89, 90] or using a linear prior in the range $[0, 10]$ eV when computing limits on Σm_ν , m_β and $m_{\beta\beta}$ ¶¶.

^{§§} The weaker preference for normal mass ordering indicated by the latest analysis of Super-Kamiokande atmospheric data will affect this result to some extent [42].

¶¶ As seen in [89], the most efficient prior for sampling the parameter space in order to obtain the mass ordering preference is the logarithmic one, which gives the same importance to all mass scales. In particular it allows us to sample uniformly the small values of m_{lightest} , which are not constrained by neutrino mass probes. Moreover, linear priors on the neutrino masses can lead to artificially stronger preferences for normal ordering [89]. However, using a linear prior on m_{lightest} is necessary in order to obtain limits on Σm_ν : i.e. having a logarithmic prior on m_{lightest} generates non-trivial distortions to the Σm_ν posterior, which remains much more peaked towards the smaller values of Σm_ν , hence precluding a simple comparison with other limits in the literature.

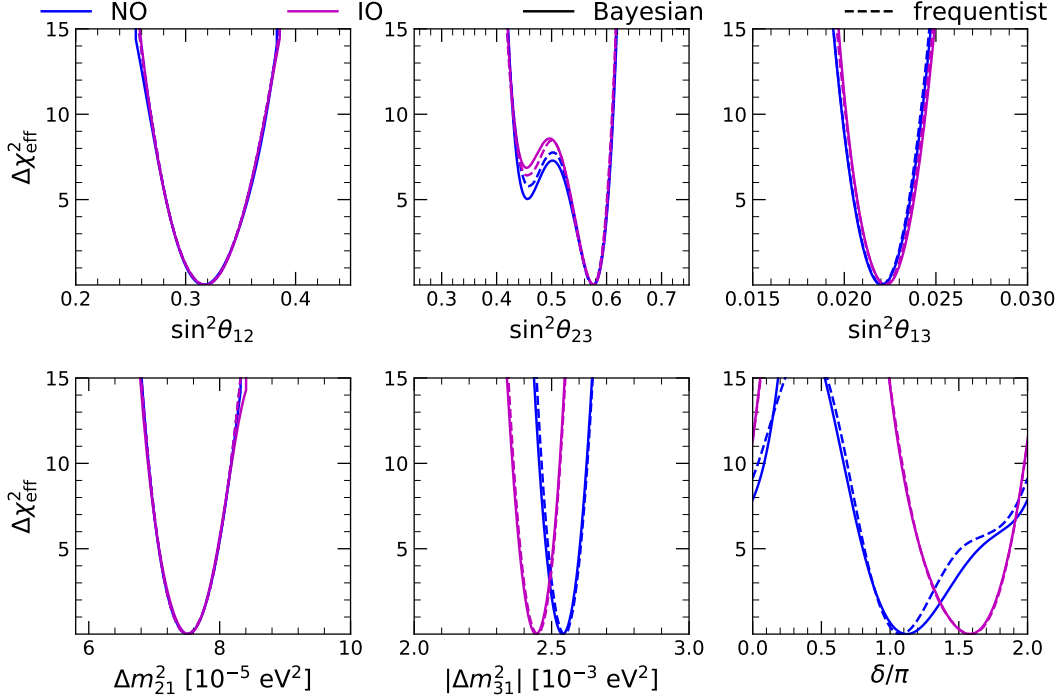


FIG. 10: Summary of neutrino oscillation parameters from our global fit, comparing the Bayesian (solid) and frequentist (dashed) determinations obtained for normal (blue) and inverted (magenta) ordering. Note that inverted ordering results are normalized with respect to the minimum χ^2 of inverted ordering.

B. Oscillation parameter results

In order to obtain a Bayesian comparison of the NO and IO spectra, we have to perform numerical analyses which we also use to produce Bayesian neutrino oscillation parameter determinations. While the likelihood is the same, converted from the χ^2 discussed in the previous sections according to Eq. (1), minor differences appear between the frequentist and Bayesian analyses, which are shown in Fig. 10. In the figure, we show the frequentist one-dimensional $\Delta\chi^2$ profiles (dashed lines) and the marginalized Bayesian posterior probabilities $P(x)$ (solid lines), converted into an effective χ^2 using

$$\Delta\chi_{\text{eff}}^2(x) = -2\log(P(x)), \quad (2)$$

where x represents any one of the six oscillation parameters. In the figure, we show NO (blue) and IO (magenta), normalizing in both cases with respect to the best fit for the same ordering of the spectrum. Apart for the normalization in the IO case, the dashed lines are the same we show in the global fit summary in Fig. 15. As we can see, most of the posterior distributions are exactly the same as the frequentist profiles. Minor differences only appear in $\sin^2\theta_{23}$ and δ , but none of the conclusions of the paper are changed.

In the first line of Tab. II and in Fig. 12, we report the significance of the Bayesian comparison of NO and IO. As we can see, the significance decreased slightly with respect to the previous results

obtained in Ref. [90], due to the mismatch in the determination of δ by T2K and NO ν A, as already explained. Neutrino oscillation data alone give now $\ln B_{\text{NO,IO}} = 3.01 \pm 0.04$, corresponding to a 2.00σ probability for a Gaussian variable.

V. ABSOLUTE SCALE OF NEUTRINO MASSES

Since neutrino oscillations depend only on the mass splittings between the neutrino mass eigenstates, in order to probe the absolute scale of the neutrino mass, other experiments are required. In this section, we discuss the status of current probes of the absolute neutrino mass: kinematic measurements through the observation of the energy spectrum of tritium β decay, neutrinoless double β decay, plus cosmological constraints.

A. The end point of β decay spectra

The kinematics of β decays can be used to probe the absolute scale of neutrino masses. Depending on the β -decaying material studied, one can access the mass of neutrinos or antineutrinos, through measurements of the electron or positron energy spectrum close to the end point. While, in principle, the electron energy spectrum contains the information encoded in each mass eigenstate, see e.g. [91], isolating the individual neutrino masses from such observations is beyond the reach of present experiments. Current β decay probes are only sensitive to the so-called effective electron neutrino mass m_β , given by the following sum:

$$m_\beta^2 = \sum_{j=1}^3 |U_{ej}|^2 m_j^2. \quad (3)$$

At the moment, the strongest limits on the effective electron antineutrino mass m_β are set by the KATRIN experiment [92], which obtained the upper limit $m_\beta < 1.1$ eV at 90% C.L.. This bound applies irrespectively of whether neutrinos are Dirac or Majorana particles. In our analysis, we do not include data from previous experiments such as MAINZ [93] and TROITSK [94], since they provide much weaker constraints than KATRIN. When performing the calculations, we take into account the KATRIN results by means of the approximated analytical likelihood proposed in Eq. (B.3) of Ref. [95]:

$$\mathcal{L}^{\text{KATRIN}} \propto \frac{1}{\sqrt{2\pi}\sigma} \exp\left(-\frac{1}{2}\left(\frac{m_\beta^2 - \mu}{\sigma}\right)^2\right) \text{erfc}\left(-\frac{\alpha}{\sqrt{2}}\frac{m_\beta^2 - \mu}{\sigma}\right), \quad (4)$$

where erfc is the complementary error function, $\sigma = 1.506$ eV², $\mu = 0.0162$ eV², $\alpha = -2.005$ and m_β^2 is in units of eV².

B. Neutrinoless double β decay

If neutrinos are Majorana particles, one expects that a neutrinoless variety of double beta decay in which no neutrinos are emitted as real particles should take place. This is called neutrinoless double β decay ($0\nu\beta\beta$) and, if it is ever detected, it implies the Majorana nature of neutrinos [96]. The non-observation of $0\nu\beta\beta$ can then be used to set complementary limits on the neutrino mass scale. The decay amplitude is given as

$$m_{\beta\beta} = \left| \sum_{j=1}^3 U_{ej}^2 m_j \right|, \quad (5)$$

where m_j are the Majorana masses of the three light neutrinos. Notice the absence of complex conjugation of the lepton mixing matrix elements. These contain the new CP phases [97, 98] characteristic of the Majorana neutrinos (note that the Dirac phase that appears in neutrino oscillations does not appear in the $0\nu\beta\beta$ amplitude). This is manifest within the original symmetrical parametrization of the lepton mixing matrix [97] in which the Majorana phases are treated symmetrically, each one associated to the corresponding mixing angles ***.

One finds that $0\nu\beta\beta$ probes constrain the half-life $T_{1/2}^{0\nu}(\mathcal{N})$ of the isotope involved in the decay (see e.g. [100] for a recent review). Assuming that the dominant mechanism responsible for the $0\nu\beta\beta$ events is light neutrino exchange, one finds constraints on $T_{1/2}^{0\nu}(\mathcal{N})$ which can be translated into bounds on the effective Majorana mass $m_{\beta\beta}$.

The conversion between half-life and effective Majorana mass is

$$T_{1/2}^{0\nu}(\mathcal{N}) = \frac{m_e^2}{G_{0\nu}^{\mathcal{N}} |\mathcal{M}_{0\nu}^{\mathcal{N}}|^2 m_{\beta\beta}^2}, \quad (6)$$

where m_e is the electron mass, $G_{0\nu}^{\mathcal{N}}$ is the phase space factor and $\mathcal{M}_{0\nu}^{\mathcal{N}}$ is the nuclear matrix element for the decay. The latter two terms depend on the isotope under consideration.

Lower limits on the half-life $T_{1/2}^{0\nu}(\mathcal{N})$ have been set by various experiments, using different isotopes, including ^{76}Ge , ^{130}Te and ^{136}Xe . The strongest bounds for these isotopes have been set, respectively, by Gerda [101] for ^{76}Ge ($T_{1/2}^{0\nu} > 9 \times 10^{25}$ yr), by CUORE [102] for ^{130}Te ($T_{1/2}^{0\nu} > 3.2 \times 10^{25}$ yr) and by KamLAND-Zen [103] for ^{136}Xe ($T_{1/2}^{0\nu} > 1.07 \times 10^{26}$ yr), all at 90% C.L. In our analyses, we consider bounds from the above-mentioned experiments using approximated analytical expressions for the three likelihoods:

$$-\ln \mathcal{L}^{\text{Gerda}} \propto -5.5 + 26.7 (T_{1/2}^{0\nu})^{-1} + 38.4 (T_{1/2}^{0\nu})^{-2}, \quad (7)$$

$$-\ln \mathcal{L}^{\text{CUORE}} \propto 4.02 + 10.5 (T_{1/2}^{0\nu})^{-1} + 8.6 (T_{1/2}^{0\nu})^{-2}, \quad (8)$$

$$-\ln \mathcal{L}^{\text{KamLAND-Zen}} \propto 9.71 (T_{1/2}^{0\nu})^{-1} + 28.1 (T_{1/2}^{0\nu})^{-2}. \quad (9)$$

*** For a detailed discussion of original ‘‘symmetrical’’ phase convention and that of the PDG, see Ref. [99]. The distinction is important if, given a positive $0\nu\beta\beta$ signal, the phases were to be extracted. For our discussion this subtlety does not matter, as the unknown Majorana phases will be marginalized over.

The latter expression was proposed in [104], while the former two have been obtained using the information from [101] and [102], respectively, and using the general fitting formula proposed in [104].

When performing analyses including constraints from neutrinoless double β decay probes, we marginalize over the two Majorana phases in their allowed range. Moreover, in order to take into account the theoretical uncertainties in the calculation of the nuclear matrix elements, we vary them within the ranges

$$\mathcal{M}_{0\nu}^{76\text{Ge}} \in [3.35, 5.75], \quad (10)$$

$$\mathcal{M}_{0\nu}^{130\text{Te}} \in [1.75, 5.09], \quad (11)$$

$$\mathcal{M}_{0\nu}^{136\text{Xe}} \in [1.49, 3.69], \quad (12)$$

which correspond to the proposed 1σ range from [105] (see Tab. 6 in that reference).

This way, we find that the bounds on the half-life $T_{1/2}^{0\nu}(\mathcal{N})$ from the three experiments under consideration imply the following upper limits on the effective mass: $m_{\beta\beta} < 104 - 228$ meV by Gerda [101], $m_{\beta\beta} < 75 - 350$ meV by CUORE [102] and $m_{\beta\beta} < 61 - 165$ meV by KamLAND-Zen [103], respectively, where the lower (upper) values correspond to the most aggressive (conservative) choices for the nuclear matrix elements.

C. Cosmological probes

Stronger, though model-dependent (see e.g. [106]), are the limits on the sum of the neutrino masses provided by cosmological observations. They arise mainly from the combination of Cosmic Microwave Background (CMB) and Baryon Acoustic Oscillation (BAO) measurements (see e.g. [107]). Due to the anticorrelation between the sum of the neutrino masses and the Hubble parameter, it is also interesting to consider constraints on the latter quantity.

In our analyses, we consider the most recent observations of the CMB spectrum by Planck [108, 109], which measures the temperature and polarization spectra in a wide range of multipoles through the respective two-point correlation functions [110] and the lensing [111] potential through the four-point correlation function. We include BAO observations from the 6dF [112], SDSS DR7 Main Galaxy Sample (MGS) [113] and BOSS DR12 [114] galaxy redshift surveys. Bounds on the expansion of the universe quantified by the Hubble parameter $H(z)$ also come from measurements at $z = 0.45$ [115]. Constraints from observations of Type Ia Supernovae are also taken into account, by means of the Pantheon sample [116]. Here we will indicate by ‘‘Cosmo’’ the combination that includes Planck CMB temperature, polarization and lensing spectra, BAO measurements, $H(z)$ observations and Supernovae luminosity distance data. Finally, the most recent determination of the Hubble parameter today, $H_0 = 74.03 \pm 1.42$ km/s/Mpc from [117], is also included in some cases in order to illustrate the impact of the $\Sigma m_\nu - H_0$ degeneracy.

The calculation of predicted cosmological observables is performed using the Boltzmann solver code CLASS [118–120]. Our fiducial cosmological model is a minimal extension of the Λ CDM

model, which is described by the usual six free parameters. Namely, the baryon and cold dark matter physical densities $\Omega_b h^2$ and $\Omega_c h^2$, the angular size of the sound horizon at last-scattering θ_s , the optical depth to reionization τ and the amplitude and tilt of the primordial scalar power spectrum A_s and n_s . We fix the number of ultra-relativistic species to zero and we add three massive neutrinos, each with its own mass. Such masses are derived from the lightest neutrino mass m_{lightest} and the two mass splittings before performing the cosmological calculations. The total neutrino mass in the two orderings reads as

$$\begin{aligned}\Sigma m_\nu^{\text{NO}} &= m_{\text{lightest}} + \sqrt{m_1^2 + \Delta m_{21}^2} + \sqrt{m_1^2 + \Delta m_{31}^2} , \\ \Sigma m_\nu^{\text{IO}} &= m_{\text{lightest}} + \sqrt{m_3^2 + |\Delta m_{31}^2|} + \sqrt{m_3^2 + |\Delta m_{31}^2| + \Delta m_{21}^2} .\end{aligned}\tag{13}$$

D. Global results on the neutrino mass scale and mass ordering

Once we add in our analyses the constraints from β decay, neutrinoless double- β decay and cosmology, we are able to obtain upper bounds on the absolute scale of neutrino masses. Here we present the results in terms of m_{lightest} , which is the quantity we can compare in an easier way when discussing the various probes. In Fig. 11 we report the constraints on m_{lightest} in a prior-independent way, using the method of Refs. [121–123] and recently revived in [124]. The plotted function

$$\mathcal{R}(m_{\text{lightest}}, 0) \equiv \frac{p(m_{\text{lightest}})/\pi(m_{\text{lightest}})}{p(m_{\text{lightest}}=0)/\pi(m_{\text{lightest}}=0)}\tag{14}$$

shows the ratio between the posterior $p(m_{\text{lightest}})$ and the prior $\pi(m_{\text{lightest}})$ normalized with respect to the same ratio computed at $m_{\text{lightest}} = 0$, for different data sets, and comparing normal (blue) to inverted (magenta) mass ordering. Such quantity, which has the property of being independent of the shape and normalization of the prior $\pi(m_{\text{lightest}})$, is statistically equivalent to a Bayes factor between a model where m_{lightest} has been fixed to some value and one where m_{lightest} is equal to zero. Since the considered measurements are insensitive to the value of m_{lightest} when it is very small, the function \mathcal{R} is expected to be equal to one for small m_{lightest} ^{†††}, while it decreases when large values of m_{lightest} become disfavored. In the same way as a Bayes factor, we can compare the constraining power of different data sets by means of the Jeffreys' scale. The horizontal lines in Fig. 11 show the values $\ln \mathcal{R} = -1, -3, -6$, which separate regions where the significance is none, weak, moderate and strong, according to the Jeffreys' scale we adopt.

Analyzing the figure, it is possible to notice that the results obtained from the β -decay data (solid) are completely insensitive to the mass ordering, and provide the weakest constraints on m_{lightest} nowadays. We must remember, however, that β decay measurements provide the most robust, less biased constraints on the absolute scale of neutrino masses, as they are completely

^{†††} Note that, due to the numerical noise in the MCMC, the posterior at small values of m_{lightest} is not perfectly stable and, as a consequence, \mathcal{R} is not exactly constant.

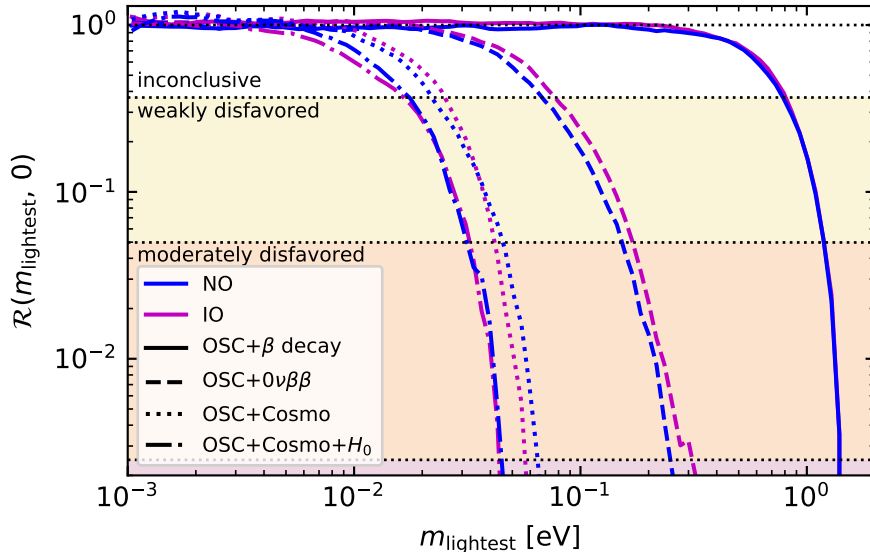


FIG. 11: Prior-independent [124] constraints on the lightest neutrino mass from different data combinations, for normal (blue) and inverted (magenta) neutrino mass ordering.

model independent. Neutrinoless double- β decay bounds (dashed), which only apply to Majorana neutrinos, provide stronger bounds, with minor differences between NO and IO, which are just due to MCMC noise. The stronger constraints on m_{lightest} come from cosmological measurements. The inclusion of a prior on H_0 [117] (dashed-dotted) further reduces the allowed range for m_{lightest} with respect to the Cosmo data set (dotted). This is a consequence of the anticorrelation between Σm_ν and H_0 , which reduces the allowed range for Σm_ν when H_0 is forced to increase by the tension between the local measurement and the value of H_0 derived from CMB observations, see e.g. [107]. To summarize, the OSC+Cosmo fit strongly disfavors values of m_{lightest} above 0.065 eV (0.058 eV), while in the OSC+Cosmo+ H_0 fit the strongly disfavored values above 0.045 eV for both mass orderings. For an easier comparison with bounds existing in literature, we also quote the marginalized limits on the sum of the neutrino masses at 2σ , computed with a linear prior on m_{lightest} , which are 0.15 eV (0.16 eV) when considering OSC+Cosmo data, while in the OSC+Cosmo+ H_0 fit they become 0.12 eV (0.15 eV), for NO (IO). Notice that the NO and IO bounds differ, and in both cases these results are less constraining than those obtained by the Planck collaboration and in Refs. [125–127] after considering very similar cosmological observations. Namely, in Ref. [109] it is quoted $\Sigma m_\nu < 0.12$ eV from CMB temperature, polarization, lensing and BAO observations. This is due to the different lower prior assumed in our global fit: while the Planck collaboration just assumes a physical prior on the sum of the neutrino masses, i.e. $\Sigma m_\nu > 0$, here the lower value of the prior is determined by neutrino oscillation experiments assuming $m_{\text{lightest}} = 0$, and it is therefore different for NO and IO. We refer to reader to Ref. [126] and Ref. [106] for an assessment of the changes in the upper bounds on the total neutrino mass after taking into account neutrino oscillation information and the uncertainty on the underlying

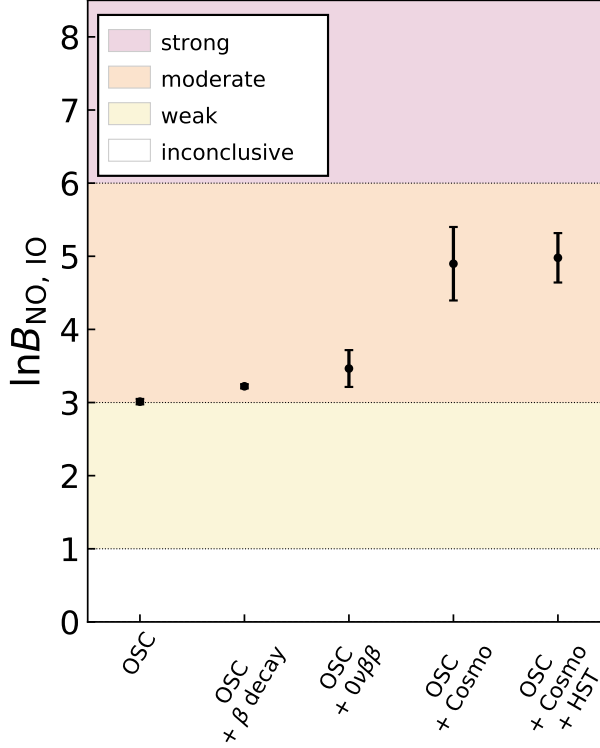


FIG. 12: Bayes factors comparing normal and inverted neutrino mass ordering, using oscillation data alone and in combination with other data sets sensitive to the absolute scale of neutrino masses.

data set	$\ln B_{\text{NO},10}$	$N\sigma$
OSC	3.01 ± 0.04	2.00
OSC + β decay	3.22 ± 0.03	2.07
OSC + $0\nu\beta\beta$	3.46 ± 0.25	2.17
OSC + Cosmo	4.90 ± 0.50	2.68
OSC + Cosmo + H_0	4.98 ± 0.34	2.70

TABLE II: Bayes factors and significance in terms of standard errors of normal versus inverted mass ordering for various data combinations.

cosmological model, respectively.

Considering absolute neutrino mass measurements also affects the preference in favor of NO previously reported from oscillation data only. While the strength of β decay constraints is not yet sufficient to discriminate the mass ordering, in the case of Majorana neutrinos, the bounds obtained by $0\nu\beta\beta$ experiments provide some additional significance in favor of NO, from 2.00σ (oscillations only) to 2.17σ , as reported in Tab. II and Fig. 12. The significance increases even more when the constraints on the neutrino mass from cosmology are taken into account. In such case, we obtain a preference of $\sim 2.68\sigma$ when considering oscillation data plus the Cosmo set, which does not vary significantly if a prior on the Hubble parameter is also included. The stronger preference obtained in favor of NO in such cases is due to the fact that cosmology puts stronger

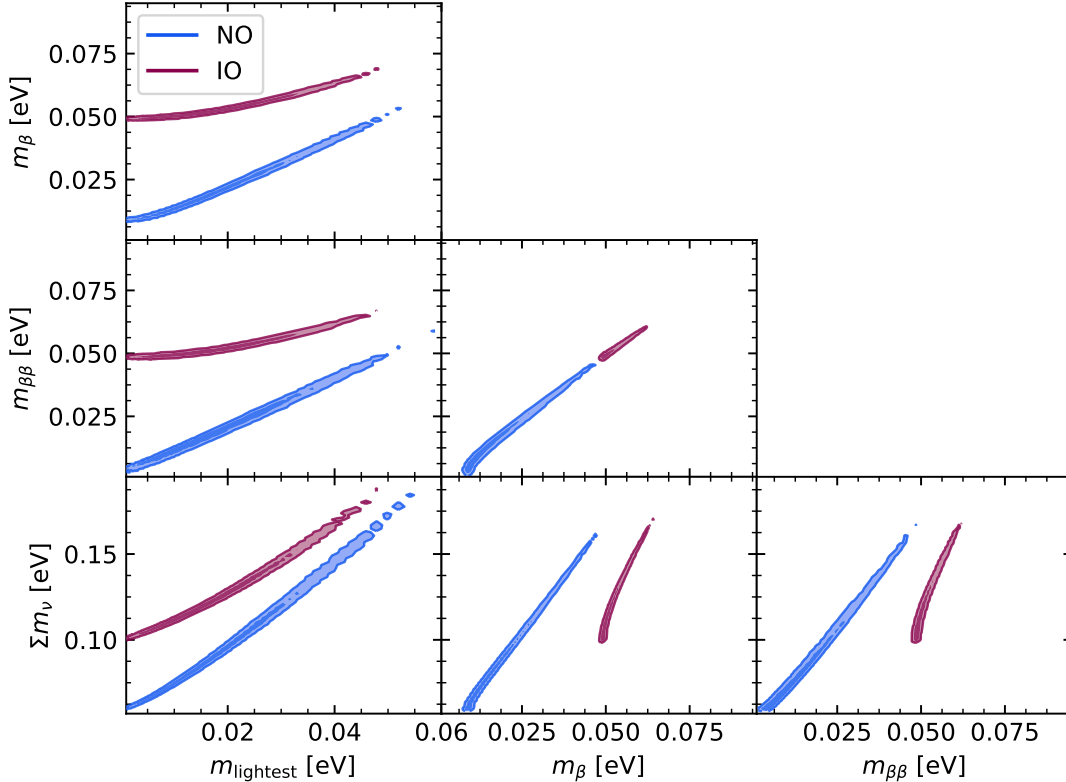


FIG. 13: Marginalized allowed regions at 1σ (dark area) and 2σ (light area) for m_{lightest} , m_β , $m_{\beta\beta}$ and Σm_ν , obtained considering the data combination we denote as OSC+Cosmo, for NO (blue) and IO (magenta).

constraints on the absolute scale of neutrino masses. In the IO case, stronger bounds on Σm_ν result in a smaller available parameter space volume, since the minimum allowed value for Σm_ν is bounded from below by ~ 0.1 eV instead of the ~ 0.06 eV that apply for NO, which is therefore preferred.

Finally, we report in Fig. 13 the allowed regions at 1, 2σ for the mass parameters m_{lightest} , m_β , $m_{\beta\beta}$ and Σm_ν obtained considering the OSC+Cosmo data set. We do not show the regions allowed by β -decay and $0\nu\beta\beta$ experiments as they are outside the scale of the respective effective parameter: in other words, the constraints that we obtain considering cosmological data are much tighter than those obtained from terrestrial experiments (see Secs. VA and VB).

VI. SUMMARY OF THE GLOBAL FIT

In this study we have first analyzed global data coming only from neutrino oscillation experiments. These hold in complete generality. In a second step, we have combined the oscillation results with direct neutrino mass probes such as β decay, neutrinoless double β decay and cosmological observations. The latter has its caveats, for example, $0\nu\beta\beta$ restrictions apply only to Majorana neutrinos, while cosmological considerations suffer from a higher degree of model-dependence.

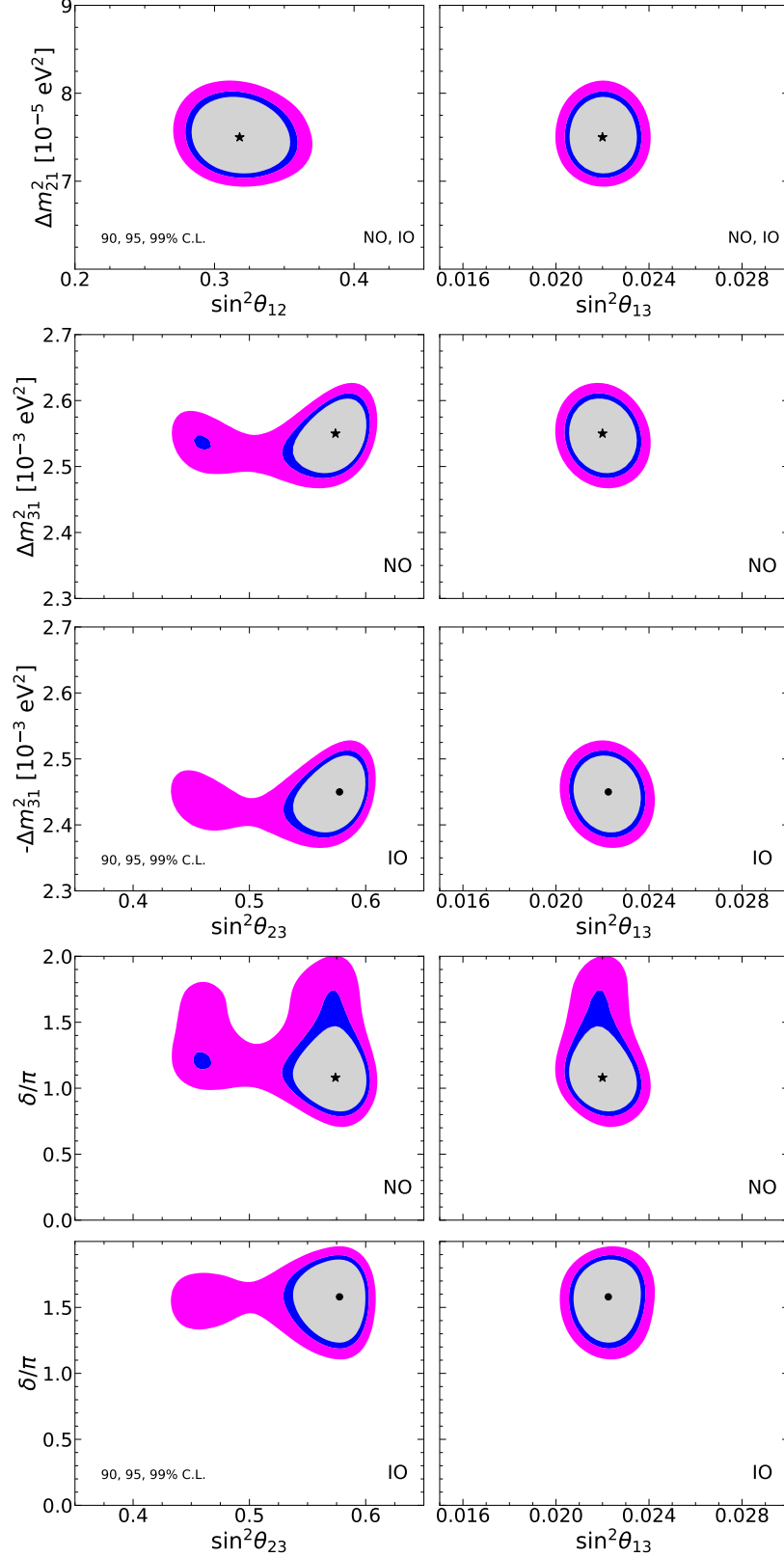


FIG. 14: Overall summary of our global fit to neutrino oscillation data. Global fit regions correspond to 90, 95 and 99% C.L. (2 d.o.f.). Regions for inverted ordering are plotted with respect to the local minimum in this neutrino mass ordering. The absolute minimum corresponding to NO is indicated by a star, while the local minimum in IO is denoted by a black dot.

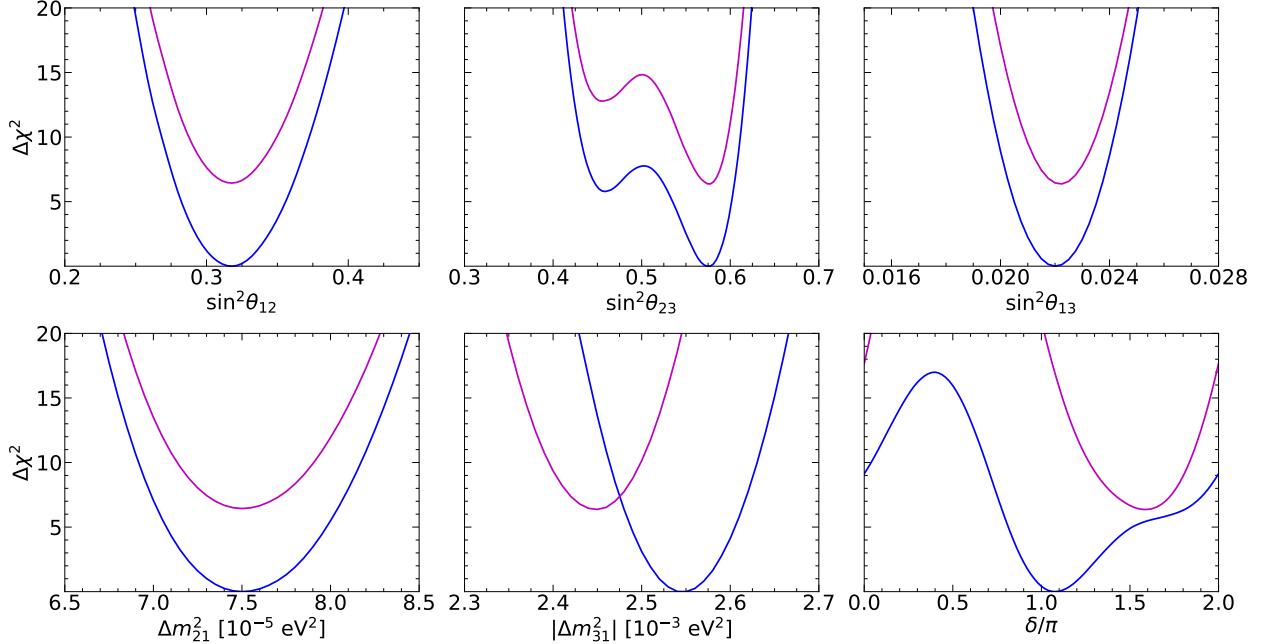


FIG. 15: Overall summary of neutrino oscillation parameter determinations. Blue lines correspond to NO and magenta lines to IO.

The results from our frequentist global fit to neutrino oscillation data are summarized in Figs. 14 and 15 and in Tab. III. We have reanalyzed SNO data obtaining now a more constraining upper bound on the solar mixing angle $\sin^2 \theta_{12}$ than that obtained in the recent global fit, Ref. [1], with the new best fit value slightly smaller. While the determination of the solar mass splitting Δm_{21}^2 remains unchanged, the best fit value is also smaller than that obtained before. Due to new short-baseline reactor data from Daya Bay and RENO, we obtain an improved measurement of $\sin^2 \theta_{13}$ and a larger best fit value of $\sin^2 \theta_{13} = 0.0220$. Also the best fit value of the atmospheric mass splitting Δm_{31}^2 is now larger, with a slightly better determination. Regarding the atmospheric angle, we obtain the best fit value $\sin^2 \theta_{23} = 0.574$ (0.578) for normal (inverted) ordering. Indeed, the preference for the second octant obtained here is stronger than in Ref. [1], and lower octant solutions are now disfavored with $\Delta\chi^2 \geq 5.8$ (6.4) for normal (inverted) ordering.

However, for the case of the CP-violating phase δ , we obtain a weaker result in comparison with our previous global fit [1], due to the mismatch in the value of δ extracted by T2K and NO ν A. The best fit is obtained for $\delta = 1.08\pi$ (1.58π) for normal (inverted) ordering. Concerning the CP-conserving values, $\delta = 0$ is disfavored with $\Delta\chi^2 = 9.1$ (11.3) for NO (IO), while $\delta = \pi$, remains allowed with $\Delta\chi^2 = 0.4$ for NO and it is excluded with $\Delta\chi^2 = 14.6$ in IO. This is due to the fact that the aforementioned mismatch in the extracted value of δ by the T2K and NO ν A experiments only occurs for normal ordering. Indeed, for inverted mass ordering both experiments prefer values close to maximal CP violation, with $\delta \approx 1.5\pi$. Finally, the very same mismatch reduces the statistical significance of the preference for NO from the 3.4σ obtained in Ref. [1] to the 2.5σ derived in the frequentist analysis presented in this work.

parameter	best fit $\pm 1\sigma$	2σ range	3σ range
$\Delta m_{21}^2 [10^{-5} \text{eV}^2]$	$7.50^{+0.22}_{-0.20}$	7.12–7.93	6.94–8.14
$ \Delta m_{31}^2 [10^{-3} \text{eV}^2]$ (NO)	$2.55^{+0.02}_{-0.03}$	2.49–2.60	2.47–2.63
$ \Delta m_{31}^2 [10^{-3} \text{eV}^2]$ (IO)	$2.45^{+0.02}_{-0.03}$	2.39–2.50	2.37–2.53
$\sin^2 \theta_{12}/10^{-1}$	3.18 ± 0.16	2.86–3.52	2.71–3.69
$\theta_{12}/^\circ$	34.3 ± 1.0	32.3–36.4	31.4–37.4
$\sin^2 \theta_{23}/10^{-1}$ (NO)	5.74 ± 0.14	5.41–5.99	4.34–6.10
$\theta_{23}/^\circ$ (NO)	49.26 ± 0.79	47.37–50.71	41.20–51.33
$\sin^2 \theta_{23}/10^{-1}$ (IO)	$5.78^{+0.10}_{-0.17}$	5.41–5.98	4.33–6.08
$\theta_{23}/^\circ$ (IO)	$49.46^{+0.60}_{-0.97}$	47.35–50.67	41.16–51.25
$\sin^2 \theta_{13}/10^{-2}$ (NO)	$2.200^{+0.069}_{-0.062}$	2.069–2.337	2.000–2.405
$\theta_{13}/^\circ$ (NO)	$8.53^{+0.13}_{-0.12}$	8.27–8.79	8.13–8.92
$\sin^2 \theta_{13}/10^{-2}$ (IO)	$2.225^{+0.064}_{-0.070}$	2.086–2.356	2.018–2.424
$\theta_{13}/^\circ$ (IO)	$8.58^{+0.12}_{-0.14}$	8.30–8.83	8.17–8.96
δ/π (NO)	$1.08^{+0.13}_{-0.12}$	0.84–1.42	0.71–1.99
$\delta/^\circ$ (NO)	194^{+24}_{-22}	152–255	128–359
δ/π (IO)	$1.58^{+0.15}_{-0.16}$	1.26–1.85	1.11–1.96
$\delta/^\circ$ (IO)	284^{+26}_{-28}	226–332	200–353

TABLE III: Neutrino oscillation parameters summary determined from the global analysis. The ranges for inverted ordering refer to the local minimum for this neutrino mass ordering.

Our results from the Bayesian analysis are summarized in Fig. 12 and Tab. II. Performing the Bayesian analysis, we obtain a Bayes factor of $\ln B = 3.01 \pm 0.04$ in favor of normal neutrino mass ordering from neutrino oscillation data alone. This would correspond to a Gaussian preference of 2.00σ . The determination of neutrino oscillation parameters shows also an excellent agreement among the frequentist and Bayesian analyses.

While the inclusion of β -decay data basically does not change the former Bayes factor, data from $0\nu\beta\beta$ experiments mildly increase that figure to $\ln B = 3.46 \pm 0.25$, now indicating moderate preference for normal neutrino mass ordering. Note, however, that this improvement would only apply if neutrinos are Majorana particles. The combination with data from cosmological observations is independent of the neutrino nature and leads to a Bayes factor of $\ln B = 4.90 \pm 0.50$, still moderately preferring normal neutrino mass ordering and corresponding to a statistical significance of 2.68σ . Finally, when we also include in the cosmological observations a prior on the Hubble constant we obtain $\ln B = 4.98 \pm 0.34$, corresponding to a preference for NO of 2.70σ .

Concerning the cosmological limits on the sum of the neutrino masses, the tightest 2σ bound we obtain here is $\sum m_\nu < 0.12$ (0.15) eV for NO (IO) taking into account CMB temperature, polarization and lensing measurements from the Planck satellite, BAO observations, $H(z)$ information and Supernovae Ia data. These limits are slightly weaker than those existing in the literature due

to our prior, that takes into account neutrino oscillation results as an input.

Overall, we have seen that the determination of some of the neutrino parameters has improved thanks to new oscillation data, while the determination of δ and the neutrino mass ordering has worsened, due to a new tension in current long-baseline accelerator measurements. We have also seen that the inclusion of non-oscillation data, especially from cosmological observations, enhances the preference for normal neutrino mass ordering from “almost weak” to “moderate”.

In summary, neutrino oscillation parameters are currently measured with very good precision. In the upcoming years these accurate measurements will further improve, allowing for better sensitivities to New Physics effects, which may show up as sub-leading effects in the neutrino oscillation probabilities.

Acknowledgments

We thank Chad Finley from the IceCube collaboration for useful comments on the IceCube DeepCore analysis. We are very grateful to Soo-Bong Kim from the RENO collaboration for providing the digitized data for 2900 days of running time. Work supported by the Spanish grants FPA2017-85216-P and FPA2017-85985-P (AEI/FEDER, UE), PROMETEO/2018/165 and PROMETEO/2019/083 (Generalitat Valenciana) and the Red Consolider MultiDark FPA2017-90566-REDC. PFdS acknowledges support by the Vetenskapsrådet (Swedish Research Council) through contract No. 638-2013-8993 and the Oskar Klein Centre for Cosmoparticle Physics. DVF acknowledges the financial support of UdeM under the internal call, number 48, “proyectos de investigación en colaboración” project 1117 and thanks A. Tapia for useful discussions. SG acknowledges financial support by the “Juan de la Cierva-Incorporación” program (IJC2018-036458-I) of the Spanish MINECO, until September 2020, and by the European Union’s Horizon 2020 research and innovation programme under the Marie Skłodowska-Curie grant agreement No 754496 (project FELLINI) starting from October 2020. PMM acknowledges financial support from the FPU grant FPU18/04571. OM is also supported by the European Union Horizon 2020 research and innovation program (grant agreements No. 690575 and 67489). CAT is supported by the FPI grant BES-2015-073593 and by the research grant “The Dark Universe: A Synergic Multimessenger Approach” number 2017X7X85K under the program “PRIN 2017” funded by the Ministero dell’Istruzione, Università e della Ricerca (MIUR). MT acknowledges financial support from MINECO through the Ramón y Cajal contract RYC-2013-12438.

-
- [1] P. F. de Salas, D. V. Forero, C. A. Ternes, M. Tórtola, and J. W. F. Valle, “Status of neutrino oscillations 2018: 3σ hint for normal mass ordering and improved CP sensitivity,” *Phys. Lett. B* **782** (Jul, 2018) 633–640, [arXiv:1708.01186 \[hep-ph\]](#).
 - [2] D. V. Forero, M. Tortola, and J. W. F. Valle, “Neutrino oscillations refitted,” *Phys.Rev.D* **90** no. 9, (2014) 093006, [arXiv:1405.7540 \[hep-ph\]](#).

- [3] D. V. Forero, M. Tortola, and J. W. F. Valle, “Global status of neutrino oscillation parameters after Neutrino-2012,” *Phys. Rev.* **D86** (2012) 073012, [arXiv:1205.4018 \[hep-ph\]](#).
- [4] T. Schwetz, M. Tortola, and J. W. F. Valle, “Where we are on θ_{13} : addendum to ‘Global neutrino data and recent reactor fluxes: status of three-flavour oscillation parameters’,” *New J. Phys.* **13** (2011) 109401, [arXiv:1108.1376 \[hep-ph\]](#).
- [5] T. Schwetz, M. Tortola, and J. W. F. Valle, “Global neutrino data and recent reactor fluxes: status of three-flavour oscillation parameters,” *New J. Phys.* **13** (2011) 063004, [arXiv:1103.0734 \[hep-ph\]](#).
- [6] T. Schwetz, M. Tortola, and J. W. F. Valle, “Three-flavour neutrino oscillation update,” *New J. Phys.* **10** (2008) 113011, [arXiv:0808.2016 \[hep-ph\]](#).
- [7] M. Maltoni, T. Schwetz, M. A. Tortola, and J. W. F. Valle, “Status of global fits to neutrino oscillations,” *New J. Phys.* **6** (2004) 122, [arXiv:hep-ph/0405172 \[hep-ph\]](#).
- [8] M. Maltoni, T. Schwetz, M. A. Tortola, and J. W. F. Valle, “Status of three neutrino oscillations after the SNO salt data,” *Phys. Rev.* **D68** (2003) 113010, [arXiv:hep-ph/0309130 \[hep-ph\]](#).
- [9] I. Esteban, M. Gonzalez-Garcia, M. Maltoni, T. Schwetz, and A. Zhou, “The fate of hints: updated global analysis of three-flavor neutrino oscillations,” *JHEP* **09** (2020) 178, [arXiv:2007.14792 \[hep-ph\]](#).
- [10] F. Capozzi, E. Di Valentino, E. Lisi, A. Marrone, A. Melchiorri, and A. Palazzo, “Addendum to: Global constraints on absolute neutrino masses and their ordering,” [arXiv:2003.08511 \[hep-ph\]](#).
- [11] **SNO** Collaboration, Q. Ahmad *et al.*, “Direct evidence for neutrino flavor transformation from neutral current interactions in the Sudbury Neutrino Observatory,” *Phys.Rev.Lett.* **89** (2002) 011301, [nucl-ex/0204008](#).
- [12] **Super-Kamiokande** Collaboration, Y. Fukuda *et al.*, “Evidence for oscillation of atmospheric neutrinos,” *Phys.Rev.Lett.* **81** (1998) 1562–1567, [hep-ex/9807003](#).
- [13] A. B. McDonald, “Nobel Lecture: The Sudbury Neutrino Observatory: Observation of flavor change for solar neutrinos,” *Rev.Mod.Phys.* **88** no. 3, (2016) 030502.
- [14] T. Kajita, “Nobel Lecture: Discovery of atmospheric neutrino oscillations,” *Rev.Mod.Phys.* **88** no. 3, (2016) 030501.
- [15] **KamLAND** Collaboration, K. Eguchi *et al.*, “First results from KamLAND: Evidence for reactor anti-neutrino disappearance,” *Phys.Rev.Lett.* **90** (2003) 021802, [hep-ex/0212021](#).
- [16] O. Miranda, C. Pena-Garay, T. Rashba, V. Semikoz, and J. Valle, “The Simplest resonant spin flavor solution to the solar neutrino problem,” *Nucl. Phys. B* **595** (2001) 360–380, [arXiv:hep-ph/0005259](#).
- [17] O. Miranda, C. Pena-Garay, T. Rashba, V. Semikoz, and J. Valle, “A Nonresonant dark side solution to the solar neutrino problem,” *Phys. Lett. B* **521** (2001) 299–307, [arXiv:hep-ph/0108145](#).
- [18] J. Barranco, O. Miranda, T. Rashba, V. Semikoz, and J. Valle, “Confronting spin flavor solutions of the solar neutrino problem with current and future solar neutrino data,” *Phys.Rev.* **D66** (2002) 093009, [hep-ph/0207326](#).
- [19] M. Gonzalez-Garcia, M. Guzzo, P. Krastev, H. Nunokawa, O. Peres, V. Pleitez, J. Valle, and R. Zukanovich Funchal, “Atmospheric neutrino observations and flavor changing interactions,” *Phys. Rev. Lett.* **82** (1999) 3202–3205, [arXiv:hep-ph/9809531](#).
- [20] M. Guzzo, P. de Holanda, M. Maltoni, H. Nunokawa, M. Tortola, and J. W. F. Valle, “Status of a hybrid three neutrino interpretation of neutrino data,” *Nucl.Phys.* **B629** (2002) 479–490, [hep-ph/0112310](#).
- [21] O. G. Miranda, M. A. Tortola, and J. W. F. Valle, “Are solar neutrino oscillations robust?,” *JHEP*

- 10 (2006) 008, [hep-ph/0406280](#).
- [22] I. Esteban, M. Gonzalez-Garcia, M. Maltoni, I. Martinez-Soler, and J. Salvado, “Updated Constraints on Non-Standard Interactions from Global Analysis of Oscillation Data,” *JHEP* **08** (2018) 180, [arXiv:1805.04530 \[hep-ph\]](#).
- [23] P. B. Dev *et al.*, “Neutrino Non-Standard Interactions: A Status Report,” *SciPost Phys.Proc.* **2** (2019) 001, [arXiv:1907.00991 \[hep-ph\]](#).
- [24] S. Gariazzo, C. Giunti, M. Laveder, Y. F. Li, and E. M. Zavanin, “Light sterile neutrinos,” *J.Phys.G* **43** (2016) 033001, [arXiv:1507.08204 \[hep-ph\]](#).
- [25] S. Gariazzo, C. Giunti, M. Laveder, and Y. F. Li, “Updated Global 3+1 Analysis of Short-BaseLine Neutrino Oscillations,” *JHEP* **06** (2017) 135, [arXiv:1703.00860 \[hep-ph\]](#).
- [26] M. Dentler, A. Hernández-Cabezudo, J. Kopp, P. A. Machado, M. Maltoni, I. Martinez-Soler, and T. Schwetz, “Updated Global Analysis of Neutrino Oscillations in the Presence of eV-Scale Sterile Neutrinos,” *JHEP* **08** (2018) 010, [arXiv:1803.10661 \[hep-ph\]](#).
- [27] M. Dentler, A. Hernández-Cabezudo, J. Kopp, M. Maltoni, and T. Schwetz, “Sterile Neutrinos or Flux Uncertainties? - Status of the Reactor Anti-Neutrino Anomaly,” *JHEP* **11** (2017) 099, [arXiv:1709.04294 \[hep-ph\]](#).
- [28] S. Gariazzo, C. Giunti, M. Laveder, and Y. F. Li, “Model-Independent $\bar{\nu}_e$ Short-Baseline Oscillations from Reactor Spectral Ratios,” *Phys.Lett.* **B782** (2018) 13–21, [arXiv:1801.06467 \[hep-ph\]](#).
- [29] A. Diaz, C. Argüelles, G. Collin, J. Conrad, and M. Shaevitz, “Where Are We With Light Sterile Neutrinos?,” *Phys. Rept.* **884** (2020) 1–59, [arXiv:1906.00045 \[hep-ex\]](#).
- [30] C. Giunti and T. Lasserre, “eV-scale Sterile Neutrinos,” *Ann.Rev.Nucl.Part.Sci.* **69** no. 1, (2019) 163–190, [arXiv:1901.08330 \[hep-ph\]](#).
- [31] S. Böser, C. Buck, C. Giunti, J. Lesgourgues, L. Ludhova, S. Mertens, A. Schukraft, and M. Wurm, “Status of Light Sterile Neutrino Searches,” *Prog. Part. Nucl. Phys.* **111** (2020) 103736, [arXiv:1906.01739 \[hep-ex\]](#).
- [32] B. Cleveland *et al.*, “Measurement of the solar electron neutrino flux with the Homestake chlorine detector,” *Astrophys.J.* **496** (1998) 505–526.
- [33] F. Kaether, W. Hampel, G. Heusser, J. Kiko, and T. Kirsten, “Reanalysis of the GALLEX solar neutrino flux and source experiments,” *Phys.Lett.B* **685** (2010) 47–54, [arXiv:1001.2731 \[hep-ex\]](#).
- [34] **SAGE** Collaboration, J. N. Abdurashitov *et al.*, “Measurement of the solar neutrino capture rate with gallium metal. III: Results for the 2002–2007 data-taking period,” *Phys.Rev.C* **80** (2009) 015807, [arXiv:0901.2200 \[nucl-ex\]](#).
- [35] G. Bellini *et al.*, “Precision measurement of the ^7Be solar neutrino interaction rate in Borexino,” *Phys. Rev. Lett.* **107** (2011) 141302, [arXiv:1104.1816 \[hep-ex\]](#).
- [36] **Borexino** Collaboration, G. Bellini *et al.*, “Final results of Borexino Phase-I on low energy solar neutrino spectroscopy,” *Phys.Rev.D* **89** (2014) 112007, [arXiv:1308.0443 \[hep-ex\]](#).
- [37] **Super-Kamiokande** Collaboration, J. Hosaka *et al.*, “Solar neutrino measurements in super-Kamiokande-I,” *Phys.Rev.D* **73** (2006) 112001, [arXiv:hep-ex/0508053 \[hep-ex\]](#).
- [38] **Super-Kamiokande** Collaboration, J. Cravens *et al.*, “Solar neutrino measurements in Super-Kamiokande-II,” *Phys.Rev.D* **78** (2008) 032002, [arXiv:0803.4312 \[hep-ex\]](#).
- [39] **Super-Kamiokande** Collaboration, K. Abe *et al.*, “Solar neutrino results in Super-Kamiokande-III,” *Phys.Rev.D* **83** (2011) 052010, [arXiv:1010.0118 \[hep-ex\]](#).
- [40] Y. Nakano, “PhD Thesis, University of Tokyo.”
http://www-sk.icrr.u-tokyo.ac.jp/sk/_pdf/articles/2016/doc_thesis_naknao.pdf, 2016.

- [41] G. Ranucci, “First detection of solar neutrinos from CNO cycle with Borexino,” June, 2020. <https://doi.org/10.5281/zenodo.4134014>.
- [42] Y. Nakajima, “Recent results and future prospects from Super- Kamiokande,” June, 2020. <https://doi.org/10.5281/zenodo.4134680>.
- [43] **SNO** Collaboration, B. Aharmim *et al.*, “Combined Analysis of all Three Phases of Solar Neutrino Data from the Sudbury Neutrino Observatory,” *Phys. Rev. C* **88** (2013) 025501, [arXiv:1109.0763](https://arxiv.org/abs/1109.0763) [[nucl-ex](#)].
- [44] N. Vinyoles, A. M. Serenelli, F. L. Villante, S. Basu, J. Bergstrom, M. C. Gonzalez-Garcia, M. Maltoni, C. Peña-Garay, and N. Song, “A new Generation of Standard Solar Models,” *Astrophys.J.* **835** (2017) 202, [arXiv:1611.09867](https://arxiv.org/abs/1611.09867) [[astro-ph.SR](#)].
- [45] **KamLAND** Collaboration, S. Abe *et al.*, “Precision Measurement of Neutrino Oscillation Parameters with KamLAND,” *Phys. Rev. Lett.* **100** (2008) 221803, [arXiv:0801.4589](https://arxiv.org/abs/0801.4589) [[hep-ex](#)].
- [46] **KamLAND** Collaboration, A. Gando *et al.*, “Constraints on θ_{13} from A Three-Flavor Oscillation Analysis of Reactor Antineutrinos at KamLAND,” *Phys.Rev.D* **83** (2011) 052002, [arXiv:1009.4771](https://arxiv.org/abs/1009.4771) [[hep-ex](#)].
- [47] **KamLAND** Collaboration, A. Gando *et al.*, “Reactor On-Off Antineutrino Measurement with KamLAND,” *Phys. Rev. D* **88** no. 3, (2013) 033001, [arXiv:1303.4667](https://arxiv.org/abs/1303.4667) [[hep-ex](#)].
- [48] F. Escrihuela, O. Miranda, M. Tortola, and J. W. F. Valle, “Constraining nonstandard neutrino-quark interactions with solar, reactor and accelerator data,” *Phys. Rev. D* **80** (2009) 105009, [arXiv:0907.2630](https://arxiv.org/abs/0907.2630) [[hep-ph](#)]. [Erratum: *Phys.Rev.D* 80, 129908 (2009)].
- [49] P. Coloma and T. Schwetz, “Generalized mass ordering degeneracy in neutrino oscillation experiments,” *Phys.Rev. D* **94** no. 5, (2016) 055005, [arXiv:1604.05772](https://arxiv.org/abs/1604.05772) [[hep-ph](#)]. [Erratum: *Phys.Rev.D* 95, 079903 (2017)].
- [50] S. Goswami and A. Y. Smirnov, “Solar neutrinos and 1-3 leptonic mixing,” *Phys. Rev. D* **72** (2005) 053011, [arXiv:hep-ph/0411359](https://arxiv.org/abs/hep-ph/0411359).
- [51] **RENO** Collaboration, G. Bak *et al.*, “Measurement of Reactor Antineutrino Oscillation Amplitude and Frequency at RENO,” *Phys.Rev.Lett.* **121** (2018) 201801, [arXiv:1806.00248](https://arxiv.org/abs/1806.00248) [[hep-ex](#)].
- [52] **Daya Bay** Collaboration, D. Adey *et al.*, “Measurement of electron antineutrino oscillation with 1958 days of operation at Daya Bay,” *Phys.Rev.Lett.* **121** (2018) 241805, [arXiv:1809.02261](https://arxiv.org/abs/1809.02261) [[hep-ex](#)].
- [53] H. Nunokawa, S. J. Parke, and R. Zukanovich Funchal, “Another possible way to determine the neutrino mass hierarchy,” *Phys. Rev. D* **72** (2005) 013009, [arXiv:hep-ph/0503283](https://arxiv.org/abs/hep-ph/0503283) [[hep-ph](#)].
- [54] J. Hernandez-Cabezudo, S. J. Parke, and S.-H. Seo, “Constraint on the Solar dm^2 from combined Daya Bay & RENO data,” *Phys.Rev. D* **100** (2019) 113008, [arXiv:1905.09479](https://arxiv.org/abs/1905.09479) [[hep-ex](#)].
- [55] **RENO** Collaboration, S. Seo *et al.*, “Spectral Measurement of the Electron Antineutrino Oscillation Amplitude and Frequency using 500 Live Days of RENO Data,” *Phys.Rev. D* **98** (2018) 012002, [arXiv:1610.04326](https://arxiv.org/abs/1610.04326) [[hep-ex](#)].
- [56] J. Yoo, “Reno,” June, 2020. <https://doi.org/10.5281/zenodo.4123573>.
- [57] **RENO** Collaboration, J. Choi *et al.*, “Observation of Energy and Baseline Dependent Reactor Antineutrino Disappearance in the RENO Experiment,” *Phys.Rev.Lett.* **116** (2016) 211801, [arXiv:1511.05849](https://arxiv.org/abs/1511.05849) [[hep-ex](#)].
- [58] **Daya Bay** Collaboration, F. P. An *et al.*, “Improved Measurement of the Reactor Antineutrino Flux and Spectrum at Daya Bay,” *Chin.Phys.C* **41** (2017) 013002, [arXiv:1607.05378](https://arxiv.org/abs/1607.05378) [[hep-ex](#)].
- [59] **Daya Bay** Collaboration, F. P. An *et al.*, “Measurement of electron antineutrino oscillation based

- on 1230 days of operation of the Daya Bay experiment,” *Phys.Rev.D* **95** (2017) 072006, [arXiv:1610.04802 \[hep-ex\]](#).
- [60] **Super-Kamiokande** Collaboration, K. Abe *et al.*, “Atmospheric neutrino oscillation analysis with external constraints in Super-Kamiokande I-IV,” *Phys.Rev. D* **97** (2018) 072001, [arXiv:1710.09126 \[hep-ex\]](#).
- [61] **IceCube** Collaboration, M. G. Aartsen *et al.*, “Measurement of Atmospheric Neutrino Oscillations at 6-56 GeV with IceCube DeepCore,” *Phys.Rev.Lett.* **120** (2018) 071801, [arXiv:1707.07081 \[hep-ex\]](#).
- [62] M. Aartsen *et al.*, “Measurement of Atmospheric Tau Neutrino Appearance with IceCube DeepCore,” *Phys.Rev. D* **99** (2019) 032007, [arXiv:1901.05366 \[hep-ex\]](#).
- [63] **Super-Kamiokande** Collaboration, M. Jiang *et al.*, “Atmospheric Neutrino Oscillation Analysis With Improved Event Reconstruction in Super-Kamiokande IV,” *PTEP* **2019** (2019) 053F01, [arXiv:1901.03230 \[hep-ex\]](#).
- [64] <http://www-sk.icrr.u-tokyo.ac.jp/sk/publications/data/sk.atm.data.release.tar.gz>.
- [65] **IceCube** Collaboration, M. G. Aartsen *et al.*, “Determining neutrino oscillation parameters from atmospheric muon neutrino disappearance with three years of IceCube DeepCore data,” *Phys.Rev.D* **91** (2015) 072004, [arXiv:1410.7227 \[hep-ex\]](#).
- [66] **IceCube** Collaboration, “Three-year high-statistics neutrino oscillation samples.” https://icecube.wisc.edu/science/data/highstats_nuosc_3y, 2019.
- [67] Alex Himmel, “New Oscillation Results from the NOvA Experiment,” Jul, 2020. <https://doi.org/10.5281/zenodo.3959581>.
- [68] Patrick Dunne, “Latest Neutrino Oscillation Results from T2K,” Jul, 2020. <https://doi.org/10.5281/zenodo.3959558>.
- [69] **MINOS** Collaboration, P. Adamson *et al.*, “Combined analysis of ν_μ disappearance and $\nu_\mu \rightarrow \nu_e$ appearance in MINOS using accelerator and atmospheric neutrinos,” *Phys.Rev.Lett.* **112** (2014) 191801, [arXiv:1403.0867 \[hep-ex\]](#).
- [70] **K2K** Collaboration, M. Ahn *et al.*, “Measurement of Neutrino Oscillation by the K2K Experiment,” *Phys.Rev.D* **74** (2006) 072003, [hep-ex/0606032](#).
- [71] K. Abe *et al.*, “Search for Electron Antineutrino Appearance in a Long-baseline Muon Antineutrino Beam,” *Phys.Rev.Lett.* **124** (2020) 161802, [arXiv:1911.07283 \[hep-ex\]](#).
- [72] K. Abe *et al.*, “Constraint on the Matter-Antimatter Symmetry-Violating Phase in Neutrino Oscillations,” *Nature* **580** (2020) 339–344, [arXiv:1910.03887 \[hep-ex\]](#).
- [73] **T2K** Collaboration, K. Abe *et al.*, “Search for CP Violation in Neutrino and Antineutrino Oscillations by the T2K Experiment with 2.2×10^{21} Protons on Target,” *Phys. Rev. Lett.* **121** no. 17, (2018) 171802, [arXiv:1807.07891 \[hep-ex\]](#).
- [74] **NOvA** Collaboration, M. Acero *et al.*, “New constraints on oscillation parameters from ν_e appearance and ν_μ disappearance in the NOvA experiment,” *Phys.Rev. D* **98** (2018) 032012, [arXiv:1806.00096 \[hep-ex\]](#).
- [75] **NOvA** Collaboration, M. Acero *et al.*, “First measurement of neutrino oscillation parameters using neutrinos and antineutrinos by NOvA,” *Phys.Rev.Lett.* **123** (2019) 151803, [arXiv:1906.04907 \[hep-ex\]](#).
- [76] P. Huber, M. Lindner, and W. Winter, “Simulation of long-baseline neutrino oscillation experiments with GLOBES (General Long Baseline Experiment Simulator),” *Comput. Phys. Commun.* **167** (2005) 195, [arXiv:hep-ph/0407333 \[hep-ph\]](#).

- [77] P. Huber, J. Kopp, M. Lindner, M. Rolinec, and W. Winter, “New features in the simulation of neutrino oscillation experiments with GLOBES 3.0: General Long Baseline Experiment Simulator,” *Comput. Phys. Commun.* **177** (2007) 432–438, [arXiv:hep-ph/0701187](#) [hep-ph].
- [78] MINOS Collaboration, P. Adamson *et al.*, “Measurement of Neutrino and Antineutrino Oscillations Using Beam and Atmospheric Data in MINOS,” *Phys. Rev. Lett.* **110** no. 25, (2013) 251801, [arXiv:1304.6335](#) [hep-ex].
- [79] MINOS Collaboration, P. Adamson *et al.*, “Electron neutrino and antineutrino appearance in the full MINOS data sample,” *Phys. Rev. Lett.* **110** no. 17, (2013) 171801, [arXiv:1301.4581](#) [hep-ex].
- [80] K2K Collaboration, E. Aliu *et al.*, “Evidence for muon neutrino oscillation in an accelerator-based experiment,” *Phys. Rev. Lett.* **94** (2005) 081802, [arXiv:hep-ex/0411038](#).
- [81] JUNO Collaboration, F. An *et al.*, “Neutrino Physics with JUNO,” *J.Phys. G* **43** no. 3, (2016) 030401, [arXiv:1507.05613](#) [physics.ins-det].
- [82] M. A. Tórtola, G. Barenboim, and C. A. Ternes, “CPT and CP, an entangled couple,” *JHEP* **07** (2020) 155, [arXiv:2005.05975](#) [hep-ph].
- [83] K. J. Kelly, P. A. Machado, S. J. Parke, Y. F. Perez Gonzalez, and R. Zukanovich-Funchal, “Back to (Mass-)Square(d) One: The Neutrino Mass Ordering in Light of Recent Data,” [arXiv:2007.08526](#) [hep-ph].
- [84] B. Audren, J. Lesgourgues, K. Benabed, and S. Prunet, “Conservative Constraints on Early Cosmology: an illustration of the Monte Python cosmological parameter inference code,” *JCAP* **02** (2013) 001, [arXiv:1210.7183](#) [astro-ph.CO].
- [85] T. Brinckmann and J. Lesgourgues, “MontePython 3: boosted MCMC sampler and other features,” *Phys.Dark Univ.* **24** (2019) 100260, [arXiv:1804.07261](#) [astro-ph.CO].
- [86] A. Heavens *et al.*, “Marginal Likelihoods from Monte Carlo Markov Chains,” [arXiv:1704.03472](#) [stat.CO].
- [87] W. J. Handley, M. P. Hobson, and A. N. Lasenby, “PolyChord: nested sampling for cosmology,” *Mon.Not.Roy.Astron.Soc.* **450** no. 1, (2015) L61–L65, [arXiv:1502.01856](#) [astro-ph.CO].
- [88] W. J. Handley, M. P. Hobson, and A. N. Lasenby, “PolyChord: next-generation nested sampling,” *Monthly Notices of the Royal Astronomical Society* **453** no. 4, (Jun, 2015) 4384, [1506.00171](#).
- [89] S. Gariazzo, M. Archidiacono, P. F. de Salas, O. Mena, C. A. Ternes, and M. Tórtola, “Neutrino masses and their ordering: Global Data, Priors and Models,” *JCAP* **03** (2018) 011, [arXiv:1801.04946](#) [hep-ph].
- [90] P. F. De Salas, S. Gariazzo, O. Mena, C. A. Ternes, and M. Tórtola, “Neutrino Mass Ordering from Oscillations and Beyond: 2018 Status and Future Prospects,” *Front.Astron.Space Sci.* **5** (2018) 36, [arXiv:1806.11051](#) [hep-ph].
- [91] C. Giunti and C. W. Kim, *Fundamentals of Neutrino Physics and Astrophysics*. 2007.
- [92] KATRIN Collaboration, M. Aker *et al.*, “An improved upper limit on the neutrino mass from a direct kinematic method by KATRIN,” *Phys.Rev.Lett.* **123** (2019) 221802, [arXiv:1909.06048](#) [hep-ex].
- [93] C. Kraus *et al.*, “Final results from phase II of the Mainz neutrino mass search in tritium beta decay,” *Eur.Phys.J.C* **40** (2005) 447–468, [arXiv:hep-ex/0412056](#) [hep-ex].
- [94] V. Aseev *et al.*, “Measurement of the electron antineutrino mass in tritium beta decay in the Troitsk nu-mass experiment,” *Phys.Atom.Nucl.* **75** (2012) 464–478.
- [95] G.-y. Huang, W. Rodejohann, and S. Zhou, “Effective neutrino masses in KATRIN and future tritium beta-decay experiments,” *Phys.Rev. D* **101** (2020) 016003, [arXiv:1910.08332](#) [hep-ph].

- [96] J. Schechter and J. W. F. Valle, “Neutrinoless Double beta Decay in SU(2) x U(1) Theories,” *Phys.Rev.D* **25** (1982) 2951.
- [97] J. Schechter and J. W. F. Valle, “Neutrino Masses in SU(2) x U(1) Theories,” *Phys.Rev.D* **22** (1980) 2227.
- [98] J. Schechter and J. Valle, “Neutrino Oscillation Thought Experiment,” *Phys.Rev.* **D23** (1981) 1666.
- [99] W. Rodejohann and J. Valle, “Symmetrical Parametrizations of the Lepton Mixing Matrix,” *Phys.Rev.* **D84** (2011) 073011, [arXiv:1108.3484 \[hep-ph\]](#).
- [100] S. Dell’Oro, S. Marcocci, M. Viel, and F. Vissani, “Neutrinoless double beta decay: 2015 review,” *Adv.High Energy Phys.* **2016** (2016) 2162659, [arXiv:1601.07512 \[hep-ph\]](#).
- [101] **GERDA** Collaboration, M. Agostini *et al.*, “Probing Majorana neutrinos with double- β decay,” *Science* **365** (2019) 1445, [arXiv:1909.02726 \[hep-ex\]](#).
- [102] **CUORE** Collaboration, D. Adams *et al.*, “Improved Limit on Neutrinoless Double-Beta Decay in ^{130}Te with CUORE,” *Phys.Rev.Lett.* **124** (2020) 122501, [arXiv:1912.10966 \[nucl-ex\]](#).
- [103] **KamLAND-Zen** Collaboration, A. Gando *et al.*, “Search for Majorana Neutrinos near the Inverted Mass Hierarchy Region with KamLAND-Zen,” *Phys.Rev.Lett.* **117** no. 8, (2016) 082503, [arXiv:1605.02889 \[hep-ex\]](#). [Addendum: Phys. Rev. Lett.117,no.10,109903(2016)].
- [104] A. Caldwell, A. Merle, O. Schulz, and M. Totzauer, “A Global Bayesian Analysis of Neutrino Mass Data,” *Phys.Rev. D* **96** (2017) 073001, [arXiv:1705.01945 \[hep-ph\]](#).
- [105] J. Vergados, H. Ejiri, and F. Šimkovic, “Neutrinoless double beta decay and neutrino mass,” *Int.J.Mod.Phys.* **E25** (2016) 1630007, [arXiv:1612.02924 \[hep-ph\]](#).
- [106] S. Gariazzo and O. Mena, “Cosmology-marginalized approaches in Bayesian model comparison: the neutrino mass as a case study,” *Phys.Rev. D* **99** (2019) 021301, [arXiv:1812.05449 \[astro-ph.CO\]](#).
- [107] M. Lattanzi and M. Gerbino, “Status of neutrino properties and future prospects - Cosmological and astrophysical constraints,” *Front.in Phys.* **5** (2018) 70, [arXiv:1712.07109 \[astro-ph.CO\]](#).
- [108] **Planck** Collaboration, N. Aghanim *et al.*, “Planck 2018 results. I. Overview and the cosmological legacy of Planck,” *Astron. Astrophys.* **641** (2020) A1, [arXiv:1807.06205 \[astro-ph.CO\]](#).
- [109] **Planck** Collaboration, N. Aghanim *et al.*, “Planck 2018 results. VI. Cosmological parameters,” *Astron. Astrophys.* **641** (2020) A6, [arXiv:1807.06209 \[astro-ph.CO\]](#).
- [110] **Planck** Collaboration, N. Aghanim *et al.*, “Planck 2018 results. V. CMB power spectra and likelihoods,” *Astron. Astrophys.* **641** (2020) A5, [arXiv:1907.12875 \[astro-ph.CO\]](#).
- [111] **Planck** Collaboration, N. Aghanim *et al.*, “Planck 2018 results. VIII. Gravitational lensing,” *Astron. Astrophys.* **641** (2020) A8, [arXiv:1807.06210 \[astro-ph.CO\]](#).
- [112] F. Beutler, C. Blake, M. Colless, D. H. Jones, L. Staveley-Smith, L. Campbell, Q. Parker, W. Saunders, and F. Watson, “The 6dF Galaxy Survey: Baryon Acoustic Oscillations and the Local Hubble Constant,” *Mon.Not.Roy.Astron.Soc.* **416** (2011) 3017–3032, [arXiv:1106.3366 \[astro-ph.CO\]](#).
- [113] A. J. Ross, L. Samushia, C. Howlett, W. J. Percival, A. Burden, and M. Manera, “The clustering of the SDSS DR7 main Galaxy sample - I. A 4 per cent distance measure at $z = 0.15$,” *Mon.Not.Roy.Astron.Soc.* **449** no. 1, (2015) 835–847, [arXiv:1409.3242 \[astro-ph.CO\]](#).
- [114] **BOSS** Collaboration, S. Alam *et al.*, “The clustering of galaxies in the completed SDSS-III Baryon Oscillation Spectroscopic Survey: cosmological analysis of the DR12 galaxy sample,” *Mon.Not.Roy.Astron.Soc.* **470** (2017) 2617–2652, [arXiv:1607.03155 \[astro-ph.CO\]](#).
- [115] M. Moresco, L. Pozzetti, A. Cimatti, R. Jimenez, C. Maraston, L. Verde, D. Thomas, A. Citro, R. Tojeiro, and D. Wilkinson, “A 6% measurement of the Hubble parameter at $z \sim 0.45$: direct

- evidence of the epoch of cosmic re-acceleration,” *JCAP* **05** no. 05, (2016) 014, [arXiv:1601.01701 \[astro-ph.CO\]](#).
- [116] D. M. Scolnic *et al.*, “The Complete Light-curve Sample of Spectroscopically Confirmed SNe Ia from Pan-STARRS1 and Cosmological Constraints from the Combined Pantheon Sample,” *Astrophys. J.* **859** no. 2, (2018) 101, [arXiv:1710.00845 \[astro-ph.CO\]](#).
- [117] A. G. Riess, S. Casertano, W. Yuan, L. M. Macri, and D. Scolnic, “Large Magellanic Cloud Cepheid Standards Provide a 1% Foundation for the Determination of the Hubble Constant and Stronger Evidence for Physics beyond Λ CDM,” *Astrophys. J.* **876** (2019) 85, [arXiv:1903.07603 \[astro-ph.CO\]](#).
- [118] J. Lesgourgues and T. Tram, “Fast and accurate CMB computations in non-flat FLRW universes,” *JCAP* **09** no. 09, (2014) 032, [arXiv:1312.2697 \[astro-ph.CO\]](#).
- [119] D. Blas, J. Lesgourgues, and T. Tram, “The Cosmic Linear Anisotropy Solving System (CLASS) II: Approximation schemes,” *JCAP* **07** (2011) 034, [arXiv:1104.2933 \[astro-ph.CO\]](#).
- [120] J. Lesgourgues, “The Cosmic Linear Anisotropy Solving System (CLASS) I: Overview,” [arXiv:1104.2932 \[astro-ph.IM\]](#).
- [121] P. Astone and G. D’Agostini, “Inferring the intensity of Poisson processes at the limit of the detector sensitivity (with a case study on gravitational wave burst search),” *Annals Phys.* , [hep-ex/9909047](#).
- [122] G. D’Agostini, “Confidence limits: What is the problem? Is there the solution?,” in *Workshop on confidence limits, CERN, Geneva, Switzerland, 17-18 Jan 2000: Proceedings*, pp. 3–27. 2000. [arXiv:hep-ex/0002055 \[hep-ex\]](#).
- [123] G. D’Agostini, *Bayesian Reasoning in Data Analysis*. WORLD SCIENTIFIC, Jun, 2003. <https://doi.org/10.1142/2F5262>.
- [124] S. Gariazzo, “Constraining power of open likelihoods, made prior-independent,” *Eur. Phys. J. C* **80** no. 6, (2020) 552, [arXiv:1910.06646 \[astro-ph.CO\]](#).
- [125] S. Vagnozzi, S. Dhawan, M. Gerbino, K. Freese, A. Goobar, and O. Mena, “Constraints on the sum of the neutrino masses in dynamical dark energy models with $w(z) \geq -1$ are tighter than those obtained in Λ CDM,” *Phys.Rev.D* **98** (2018) 083501, [arXiv:1801.08553 \[astro-ph.CO\]](#).
- [126] S. Vagnozzi, E. Giusarma, O. Mena, K. Freese, M. Gerbino, S. Ho, and M. Lattanzi, “Unveiling ν secrets with cosmological data: neutrino masses and mass hierarchy,” *Phys.Rev. D* **96** (2017) 123503, [arXiv:1701.08172 \[astro-ph.CO\]](#).
- [127] E. Giusarma, M. Gerbino, O. Mena, S. Vagnozzi, S. Ho, and K. Freese, “Improvement of cosmological neutrino mass bounds,” *Phys.Rev.D* **94** no. 8, (2016) 083522, [arXiv:1605.04320 \[astro-ph.CO\]](#).